Image Cover Sheet

CLASSIFICATION	SYSTEM NUMBER
UNCLASSIFIED	502142

TITLE

THEORETICAL AND EXPERIMENTAL CHARACTERIIZATIONS OF THE IR TECHNOLOGY FOR THE DETECTION OF LOW-METAL AND NONMETALLIC BURIED LANDMINES

System Number:

Patron Number:

Requester:

Notes:

DSIS Use only:

Deliver to: FF

UNCLASSIFIED

DEFENCE RESEARCH ESTABLISHMENT
CENTRE DE RECHERCHES POUR LA DÉFENSE
VALCARTIER, QUÉBEC

DREV – R–9615

Unlimited distribution/Diffusion illimitée

THEORETICAL AND EXPERIMENTAL CHARACTERIZATIONS OF THE IR TECHNOLOGY FOR THE DETECTION OF LOW-METAL AND NONMETALLIC BURIED LANDMINES

by

J.-R. Simard

March/mars 1997

Approved by/approuvé par

Chief Scientist/Scientifique en chef

17 Feb 97

Date

SANS CLASSIFICATION

ABSTRACT

One of the greatest threats during peacekeeping operations is buried low-metal mines on roads. The Canadian Department of National Defence (DND), as many other equivalent organizations around the world, initiated important efforts to develop a multisensor teleoperated mine detection vehicle under the Improved Landmine Detection Capability (ILDC) to solve this problem. One of the sensors evaluated for this project is the IR imaging technology. This document reports the results of many trials performed during the last 1 1/2 year and models developed from these results to characterize the capabilities of this technology. The fundamental variables dictating the formation of the buried mine IR signature are identified and a monitoring technique predicting the optimum performance of the technology is proposed. From especially designed trials to simulate the scenarios addressed by the ILDC project, the detection efficiencies and the false alarm rates on packed gravel and sand roads at different times of day are measured. From these results, it is observed that the best performance is obtained at night and on packed gravel road. In addition, the performance of the technology in winterlike weather, on shady roads, and for many other external conditions of interest for the ILDC project are investigated.

RÉSUMÉ

Une des plus grandes menaces durant les opérations de maintien de la paix est la présence, sur les liens routiers, de mines enfouies contenant peu de métal. Le ministère de la Défense nationale (MDN) du Canada, à l'instar de plusieurs organismes similaires d'autres pays confrontés à ce problème, a entrepris un projet important afin de développer un véhicule télécommandé équipé de capteurs multiples. Le programme vise à améliorer la capacité de détection de mines enfouies et porte l'appellation "Improved Landmine Detection Concept (ILDC)". Une des technologies évaluées dans le cadre de ce programme est la technique d'imagerie infrarouge (IR). Ce document regroupe les résultats de plusieurs essais réalisés durant les dix-huit derniers mois et expose les modèles développés à partir de ces résultats afin d'évaluer la capacité de cette technique IR à détecter les mines enfouies contenant de faibles quantités de métal. On a identifié les variables fondamentales contribuant à la signature IR des mines enfouies et on propose une technique permettant de prédire les périodes durant lesquelles la détection est optimale. À partir d'essais élaborés spécialement pour simuler les scénarios visés par le programme ILDC, l'efficacité de la méthode de détection et le taux de fausses alarmes sur les routes de sable ou de gravier

compacté sont évalués. De ces résultats, on a observé que les performances optimales de cette technique étaient obtenues durant la nuit et sur les routes de gravier compacté. Finalement, ce document présente les performances de cette technologie dans des conditions hivernales sur des routes ombragées, ainsi que dans plusieurs autres conditions externes qui sont d'un grand intérêt pour le programme ILDC.

TABLE OF CONTENTS

EXECUTIVE SUMMARY

With the important involvement of Canada in United Nations peacekeeping operations, exposure to low-metal and nonmetallic buried landmines has been identified as the most important threat to Canadian soldiers by the Department of National Defence (DND). Already, the demining operations on communication roads caused many casualties. Moreover, an estimated 5 million mines buried in Bosnia alone [1] and 85-110 millions in 62 countries [2] contribute to emphasize the severity of the situation.

At the present time, the Canadian Forces' (CF) mine detection capability is based exclusively on the well-known electro-magnetic technology, which is inefficient against low-metal and nonmetallic buried landmines, and the hand-held prodder, which is slow, labour intensive, and shows limited detection efficiencies. Furthermore, available foreign equipments offer no better capability. In response to this situation, DND initiated an important effort to develop a teleoperated multisensor mine detection vehicle: the Improved Landmine Detection Capability (ILDC) program. This vehicle, designed with a low-ground pressure feature, is likely to support four detection technologies: Minimum Metal Mine Detection (MMMD), Ground Penetrating Radar (GPR), Thermal Neutron Activation (TNA), and InfraRed (IR) Detection. This document reports experimental and theoretical work performed during the last year and a half to evaluate the characteristics and capabilities of one of these sensors, the IR detection technology.

From the experimental results gathered to evaluate exclusively the capability of IR detection technology, two main components responsible for the formation of the IR signature of a buried mine, the heat flow between the atmosphere and the soil and the heat impedance anomaly created by the buried mine, are identified. Derived from these concepts, a prediction tool, the temperature gradient in the soil, is identified as being a valuable parameter to monitor the optimum conditions under which IR technology will perform at its best. Under these optimum conditions (night-time being the best period), detection efficiencies as high as 100 % for anti-tank mines and 75 % for antipersonnel mines were observed with a false alarm rate under 1 per 10 meters travelled. Furthermore, it was observed that IR technology could detect landmines several months after they were buried and at depths of 10 cm or less.

[1] Quoted from the journal Defence News of July 8-14, 1996: *Countermine technologies flow from increased threat* by Pat Cooper.

[2] Quoted from a May 1995 TTCP paper by H.N. Hambric from Night Vision & Electronic Sensors Directorate.

With the results reported, the author believes that IR technology should become a valuable detection tool for the ILDC project in which data fusion between technologies will improve the overall detection capability to the point where it reduces considerably the threat of low-metal and nonmetallic buried landmines on roads. The ILDC project aims at developing an XDM that would be re-engineered under external contract.

1.0 INTRODUCTION

For the last 15 years, with the increase of peacekeeping activities in countries decimated by civil wars and other social disturbances, the interest in mine detection and clearance has risen considerably. To support the international effort to solve this critical problem, the Canadian Department of National Defence (DND) has put together a team of experts to design and build a multisensor teleoperated mine detection vehicle, the Improved Landmine Detection Capability (ILDC) vehicle. One critical sensor of this vehicle is a passive infrared (IR) camera. From the recent works published by many organizations (RECON/OPTICAL Inc. (Refs. 1 and 2), Wackenhut Advanced Technology Corp. (Ref. 3), WES (Ref. 4), ERIM (Ref. 5), LLNL (Refs. 6 and 7)), it is well accepted that IR technology has good capabilities to detect metal-free buried mines. However, little has been done to quantify its detection efficiency, its sensitivity to false alarms, or its performance behaviour to surrounding natural conditions. The purpose of this document is to provide some answers to these questions. Moreover, most of the information (modelling and trials) reported has been gathered while keeping in mind the operational scenarios of interest for the ILDC program. This report is organized as follows.

In Chapter 2.0, the mechanisms behind the detection of buried landmines with an IR imager are investigated. The two main components responsible for the formation of the IR signature of a buried mine, the heat flow between the atmosphere and the soil and the heat impedance anomaly created by the buried mine, are identified. Moreover, the two types of heat impedance anomalies associated with a buried mine, the surface and volume thermal effects, are described. To represent quantitatively the interaction between the heat flow dynamism and the thermal anomaly associated with a buried mine, two models are

proposed: a general model defining the main components of the buried mine thermodynamic system and a simplified model derived from the general model and developed especially to address the operational scenarios of the ILDC program. From this simplified model, a prediction tool, the temperature gradient in the soil, is identified as a valuable parameter to monitor the optimum conditions under which IR technology will perform at its best to detect low-metal buried landmines.

Chapter 3.0 describes the instrumentation used to evaluate experimentally the characteristics of IR technology for the detection of low-metal buried mines. The technical specifications of the different IR cameras (MWIR and LWIR), as given by the manufacturers, are reported. Also, the temperature probe characterizing the heat flow between the soil and the atmosphere and the mobile platform reproducing the operational scenarios defined by the ILDC program are detailed. Finally, the material, the "Adiprene L-100" made by Uniroyal Inc., selected to build the IR surrogates is discussed.

Chapter 4.0 reports a series of trials performed to evaluate experimentally the capabilities of the IR technology to detect low-metal buried landmines on packed gravel and sand roads under different environmental conditions. This chapter is composed of two main sections. First, Section 4.1 contains static trial results in which the expected apparent temperature contrasts of a buried mine in relation with the time of day, the depth of the mine, and the geographic changes are investigated. In parallel with these measurements, the validity of the models and its derived monitoring technique proposed in Chapter 2.0 are evaluated. Second, Section 4.2 shows multiple experimental results obtained from trials designed to simulate, as close as possible, the scenarios of interest for the ILDC program. For that reason, most trials reported in this section are performed with the IR camera in movement (dynamic trials) and a human operator. With these trials, the important

parameters associated with the use of IR detection technology as the apparent temperature contrast thresholds of detection, the detection efficiencies, and the false alarm rates are evaluated. In addition, the variations of these parameters (detection efficiencies and false alarm rates) in a winterlike environment are characterized. Also in this section, the influence of specific features like shady roads, temperature gradient spatial correlations, winds, road gradings, spatial structures of the IR signatures, and the IR surrogate validity for IR detection technology are discussed. Finally, the last two sections report important results on the practicality of the technology for the ILDC program and comparative tests between the MWIR and the LWIR to detect buried landmines.

After Chapter 4.0, a discussion, in which the main questions of interest for the ILDC program are addressed, is presented. Most information provided in this section is derived from the theoretical and experimental results found in the previous chapters. Finally, a conclusion summarizing the important aspects of the detection of buried landmines by IR imaging is presented.

Occasionally in this report, specific questions of interest for the ILDC committee will be debated. In order to reduce the clumsiness of this comments for non-initiated readers, these sections will be preceded by the expression "**ILDC Notes:**". With this notice, the readers will have the possibility to read or to skip these sections depending on their interest.

A patent application for the use of the temperature gradient as a tool to predict IR contrasts of buried objects has been filed. This work was carried out at DRES between September 1994 and November 1995 under Project D6300, the Improved Landmine Detection Capability (ILDC) project.

2.0 THEORETICAL CHARACTERIZATION AND MODELLING

It is well known (Refs. 6, 8 and 9) that the use of IR technology to detect buried landmines is highly dependent on the environmental conditions and time of day. To make this technology usable for the defence community, it is then necessary to characterize its behaviour and to identify the periods during which the technology performs adequately. To achieve this goal, this chapter describes what we believe is at the origin of the formation of the IR signature of buried landmines. Moreover, two models are proposed to represent the mechanisms dictating the IR signature formation. From these models, a parameter, the temperature gradient in the soil, is identified as a tool to monitor the optimum detection periods. A method to evaluate this temperature gradient is described and has been performed in the different trials presented in Chapter 4.0.

2.1 Mechanisms Behind the IR Signature Formation of Buried Mines

To understand the basic mechanisms describing the thermal characteristics of the IR signature associated with buried mines, two main principles are identified. They are:

- uniform heat flow at the soil surface,
- uniform temperature at sufficient depth.

The first principle addresses the surfaces of soil showing equivalent optical properties (as road sections) and submitted to similar surrounding conditions (sun radiation, air temperature, etc.). Under these conditions, this principle simply states the necessary equivalence in the energy absorbed and transferred to the deeper layers for all these soil surfaces. On the other hand, the second principle is supported by the natural lateral heat diffusion which

contributes to homogenize the soil temperature with increasing depth. With these two principles, the general origin of the formation of the temperature difference between the soil surface above a buried mine and on the surrounding soil surface (which we refer to as the IR signature of the buried mine when observed with a thermal imager) is relatively simple to visualize. This temperature contrast is generated by the local increase of the heat flow resistivity created by the presence of the mine and all secondary thermal effects [3] associated with it in reaction with the heat exchange between the atmosphere and the soil. During a usual 24-hour period, this heat exchange follows a cycle (see Fig. 1). At optimum day (OD) time, sun radiation and warmer air temperature are the principal contributors to the heat transferred into the ground. At that period, the higher heat resistivity of the buried mine site will create a local increase of the temperature gradient in the soil to allow an equivalent heat flow with the surrounding soil surface. Keeping in mind the second principle, uniform temperature at sufficient depth, this implies that the soil surface above the buried mine will become warmer than the surroundings. This state is referred to as the positive temperature contrast IR signature. Through the day, the transferred heat is accumulated in the deeper layer of the soil where the temperature raises. At optimum night (ON) period, when the amount of received heat from the atmosphere is highly reduced, the stored heat of the deeper layer is redirected to the soil surface by diffusion where it is lost to the atmosphere by radiative and convection processes. During that period, the locally higher heat resistance of the buried mine site will, as during daytime, increase locally the temperature gradient to carry the same amount of heat than the surrounding soil layer, but this time in the opposite direction. In that case, once again because of the second principle, the temperature on the soil surface above the buried mine will become colder than the surroundings. This state is referred to as the negative temperature contrast IR signature. Between these two optimum

[3] These secondary thermal effects will be discussed below.

periods, there are transition periods (morning and evening transition periods) during which the heat flow changes direction. During these periods, the IR signature of a buried mine will disappear.

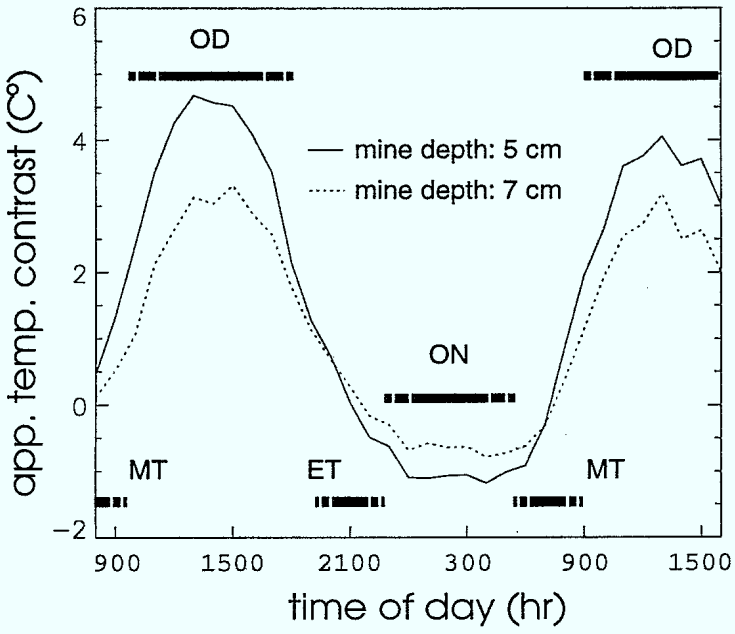

FIGURE 1 – Plot displaying the typical periodic temperature contrast evolution of two buried mines. The two mines are surrogates of the TMN-46 anti-tank mine. Four periods are clearly identifiable on this graph. The optimum day (OD) period, the optimum night (ON) period, the morning transition (MT) period, and the evening transition (ET) period. During that cycle, the transition periods are the most problematic because of the disappearance of the IR signatures associated with buried mines.

In the previous paragraph, we identified four typical periods describing the main states of the heat flow between the soil and the atmosphere. However, these cycles only represent the general behaviour of the heat dynamics between the soil and the atmosphere. In day-to-day real life, the IR signature of buried landmines will depend also on the local weather variations: arrival of a cold front, variation in cloud covers, moisture variation, and many others. A good representation of the different contributors to the heat exchange

between the soil and the atmosphere are shown in Fig. 2. On the other hand, using this representation to establish a model that will adequately allow us to predict the heat dynamic between the atmosphere-soil interface is not an easy task. Jacobs (Ref. 10) developed a model based on this representation where more than 15 parameters need to be monitored to predict adequately the temperature of a concrete slab laid on the surface of the soil. Needless to say, this approach is not compatible with the ILDC program. A method to bypass this complexity is to directly monitor the heat flow being transferred to the deeper layer of the soil. The models proposed further aim at applying this approach.

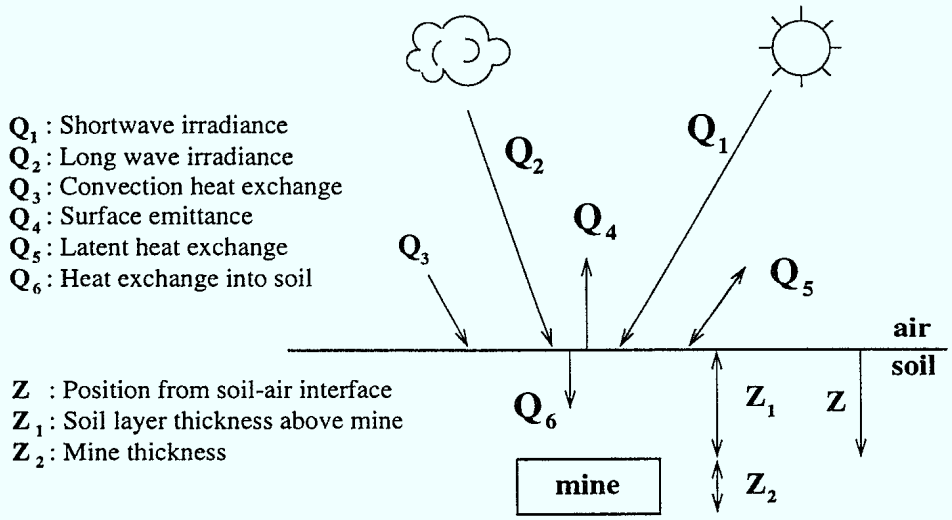

FIGURE 2 – General representation of the heat dynamic exchange between the atmosphere and the soil. Six mechanisms involved in that heat exchange are identified in this figure: the shortwave irradiance associated with sun radiation, the long wave irradiance associated with clouds and surroundings, the convection heat exchange which is related to the heat transferred between the soil and the air, the irradiation of the soil surface itself (soil surface emittance), the moisture exchange between the soil and the atmosphere (latent heat exchange), and the heat transferred to the deeper soil layer by conduction.

ILDC Notes: In a previous paragraph, we mentioned that the presence of a buried mine and associated thermal effects increases locally the soil heat impedance, which generates the IR signature of the buried mine during the heat exchange process between the atmosphere

and the soil. An interesting information representing qualitatively the impedance distortion created by the presence of the mine itself is to compare the thermal conductivity of an explosive as TNT with the usual one associated with different types of soils. From a study reported by Steinmanis (Ref. 11), we found that the thermal resistivity of more than 100 sites in Canada varies between 50 and 90°C-cm/W, which is more than seven times smaller than the heat resistivity associated with TNT (680°C-cm/W (Ref. 12)). However, it is important to mention that, even with this high heat resistivity difference between the soil and an explosive as TNT, the effective heat impedance distortion of the soil created by the presence of a buried mine alone decreases rapidly with the depth at which the mine is buried.

With all the experience accumulated with the different trials reported in Chapter 4.0, we evaluate the maximum depth at which an average size anti-tank mine can be buried before the detection of its IR signature (effect of the mine only) becomes problematic is about 10 cm. Fortunately, the heat flow distortion created by a buried mine is not only associated with the presence of the mine itself. At least for the cases of mines buried on packed gravel roads, we identified two thermal effects related to a buried landmine site which participate to the IR signature of the buried mine. They are:

- **Thermal Volume Effects**: In these effects, we include the heat impedance distortion created by the presence of the mine itself, but also the heat impedance distortion associated with the different thermal properties of the soil covering the buried mine compared with the surrounding soils. This second cause for the heat impedance of a buried mine site is referred to as the hole effect. It has been observed that the difference in compactness between the surrounding soil and the soil covering the mine creates sufficient heat impedance variation to make the IR signature of the buried mine

site detectable even if the mine itself is too deep to take an active part in the local thermal impedance distortion. This effect is also mainly responsible for the night-time IR signature of the buried mine. From the information accumulated over the different trials characterizing the IR signatures of buried mines, it has been observed that this hole effect is measurable for many months, depending upon weather conditions.

- **Thermal Surface Effects**: In opposition to the thermal volume effects, the origin of the thermal surface effect is not related at all with the presence of the buried mine. This effect appears because of the distortion of a thin layer of the soil over the buried mine site. This disturbed thin soil layer is created by the activities associated with the process of burying a mine as laying and dispersing the extra excavated soil or directly by the human actions to the soil surface during the burying operation. In reaction to these activities, a thin layer of soil with poor thermal contact with the deeper layer is created. Because of the direct exposure of this thin insulated soil layer to the atmospheric radiation (shortwave and long wave), the temperature difference between the perturbed soil surface and its immediate surroundings can reach many degrees and is easily observable with an IR imager under sunny sky. It has been observed that this surface effect is detectable for many days once again, depending upon weather conditions.

It is important to understand that buried mines are not the only cause for heat dynamic anomalies on roads. Other buried objects, highly moist road areas, vegetation (dead or alive), snow covers, shadow, or gravel artificially spread out are all sources of distortion in the heat flow mechanisms between the soil and the atmosphere, which may seriously reduce the efficiency of an IR imager to detect buried landmines. These sources of distortion can produce a high occurrence of false alarm or even hide the signs of the presence

of a buried mine. In Chapter 5.0, different sources of thermal distortion are discussed with their respective effects on the efficiency to detect buried mines on road. On the other hand, in the cases where a mine is buried in a clear area of the road and for which only the environmental conditions act on the contrast of the IR signature, there are simple models which can easily be used as thermal contrast prediction tools. These models are described in the following sections.

2.2 Simplified Model Describing the IR Signatures of Buried Mines

The simple model proposed, as the more complete one described in the following section, aims at characterizing the overall heat transfer into the ground. This approach has the advantage of bypassing the complexity associated with the thermal interaction between the atmosphere and the soil and directly monitors the physical effect responsible for the formation of the IR signature. This simple model is based on a one-dimensional thermal analysis of two soil columns: the soil column containing the buried mine and a reference soil column close by. With the introduction of the two principles mentioned in the previous section (uniform heat flow and same temperature at sufficient depth), the two soil columns can be represented as an interdependent system. Using simple electrical analogy, this system is described as two heat impedances positioned in parallel, as shown in Fig. 3. With this representation and the basic heat conduction law,

$$\Delta T = Z \times Q \qquad [1]$$

where ΔT is the temperature difference across a heat impedance Z in which exists a heat flow Q, it is quite simple to demonstrate two empirical proportionalities describing the

temperature contrast ($T_m - T_r$) on the surface of the representative soil columns:

$$(T_m - T_r) \quad \propto \quad Q, \qquad [2]$$

$$(T_m - T_r) \quad \propto \quad (Z_m - Z_r). \qquad [3]$$

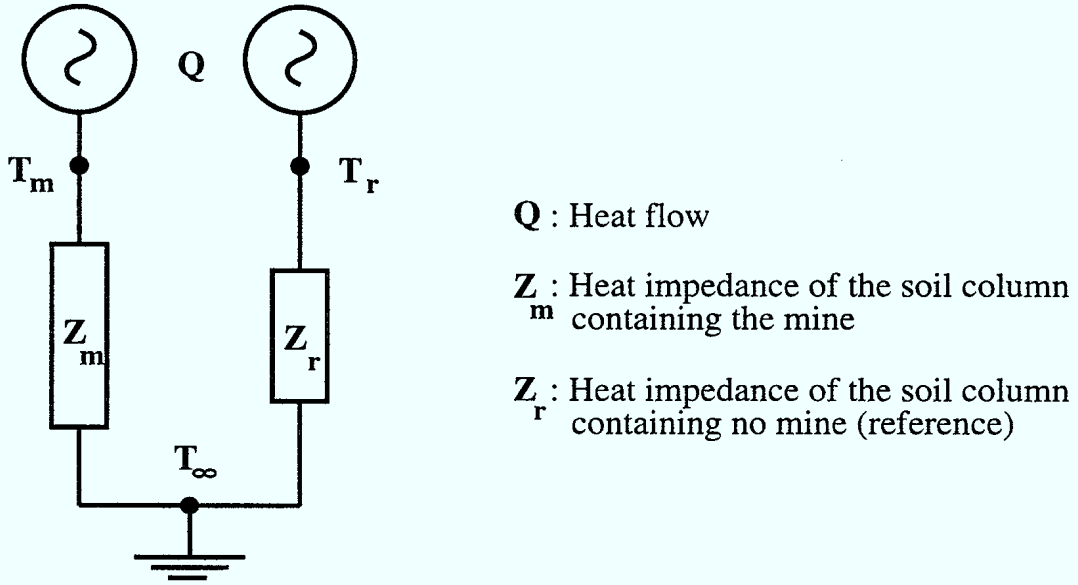

FIGURE 3 – Schematic representation of the simple model. In this model, Q is the overall heat flow between the atmosphere and the soil, T_m and T_r are the apparent temperatures on the surface of the soil where the mine is buried and on the surface of the soil column used as a reference, respectively. T_∞ is the temperature at a sufficient depth.

It is interesting to observe that these two empirical proportionalities derived from the simple model describe well the temperature contrast inversion with the change in direction of the heat and the increase of the temperature contrast with the heat impedance difference rising. It is also important to note that the first proportionality (eq. 2) opens the door to an important monitoring parameter: the heat flow into the ground (Q). From this result, it might be possible to anticipate the good and bad detection periods (or even to predict the level of the temperature contrast) associated with the general variation of the

weather conditions simply by measuring the level of heat flowing into the ground (Section 2.4 describes how the measurement of the heat flow into the ground can be done).

The simple model described here shows interesting properties associated with the behaviour of the temperature contrast of buried mines. However, this approach will not take explicitly into account the heat impedance variation associated with the depth of the buried mine or the distributed physical characteristics of the soil column. These weaknesses make difficult the applicability of the model to a real context. To reduce this difficulty, the next section shows a more complete approach to the representative model.

2.3 Detailed Model Describing the IR Signatures of Buried Mines

As mentioned in the previous section, the simple model proposed, even if it provides adequately the general thermal characteristics of a buried mine site, shows a serious weakness in its experimental application. To correct this weakness, a more detailed representation of the buried mine site is proposed. This detailed model is still based on the one-dimensional analysis of the two soil columns (the buried mine site and reference) but their spatially distributed characteristics are addressed. Figure 4 shows the two soil columns, including the depth as a variable. With this representation, a complete analytical model can be derived by solving the well-known one-dimensional differential heat equation:

$$\frac{\partial \mathrm{T}}{\partial t} = a\frac{\partial^2 \mathrm{T}}{\partial \mathrm{z}^2}, \qquad [4]$$

for the three identified zones. In this equation, T is the temperature, t is time, z is the depth, and a is the heat diffusivity defined as the ratio between the heat conductivity and the product of the heat capacity by the density. By assuming the three zones identified in

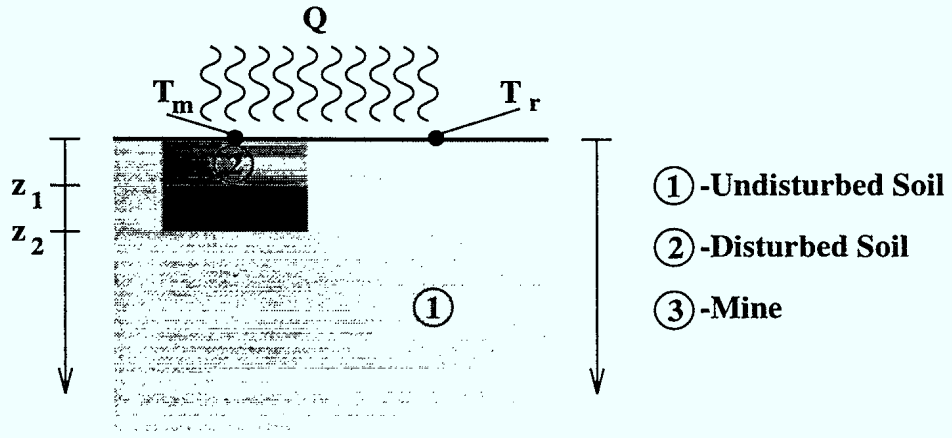

FIGURE 4 – Schematic representation of the detailed model of a buried mine site. As in the simple model shown previously, Q is the overall heat flow between the atmosphere and the soil, T_m and T_r are the apparent temperatures on the surface of the soil where the mine is buried and on the surface of the soil column used as a reference, respectively. In addition, the three zones with different thermal characteristics are identified with their spatial variable.

Fig. 4 are homogeneous [4] and by considering the heat transport by moisture migration as negligible, a complete analytical solution of the one-dimensional differential heat equation can be derived as (Ref. 13)

$$T(z,t) = T_\infty(t) + \sum_{k=1}^{\infty} A_k \exp^{-z/D} \cos(k\omega t - (z/D + \phi_k)), \qquad [5]$$

where A_k is the linear coefficient of order k of the series, D is defined as $\sqrt{2a/k\omega}$, ω is the daily thermal angular frequency and ϕ_k is a phase factor of order k. To apply this solution to the system forms by the soil column containing the buried mine and the reference soil column, eq. 5 is resolved for each zones with their associated thermal parameters and the following boundary conditions:

[4] This is not really the case, but as an approximation, we can, at first, consider the averaged thermal properties related to these zones to obtain an analytical solution. So far, this approximation appeared to be adequate for most trials.

- Continuity of the heat flow between the different zones,
- Identical temperature for the two soil columns at sufficient depth,
- Identical heat flow for the two soil columns at the atmosphere-soil interface.

There are two major advantages associated with this detailed model describing the IR signatures of the buried mines: it takes into account the depth at which the mine is buried and the thermal property variations of the soil. However, it also necessitates an adequate evaluation of many parameters defining the thermal properties of the buried mines and soils (as compactness).

ILDC Notes: At the present time, little has been done to evaluate these thermal properties for an application as the one pursued by the ILDC program. The method chosen to provide the ILDC program with an applicable model is first to evaluate the validity of the simpler approach proposed in the previous section by verifying the predicted linear relation between the heat flow into the ground and the temperature contrast of a buried mine. Then, if this relation is verified, the next step is to evaluate if the information provided by this simple model is satisfactory for the ILDC program's needs. In the case of a negative conclusion, then the more complete model proposed here should be evaluated further. However, the reader should not forget that the two models proposed aim at predicting the IR contrasts of buried mines in function of the general environmental conditions under spatially homogeneous soil surfaces. It is anticipated that any effect reducing the validity of these basic conditions (moisture inhomogeneities, shadow, partial grass cover, etc.) will degrade the predictions of the model.

2.4 Contrast Predictions Using the Simple Model

In Section 2.2, a linear relation was identified between the temperature contrast of a buried mine and the heat flow into the ground. As a consequence, the use of that relation to predict the IR signature of a buried mine necessitates a method to monitor that heat flow. This can be done by applying once again a basic law of thermodynamic stating that

$$Q \propto \frac{\partial T}{\partial z}. \qquad [6]$$

This relation is usually applied to the case of the heat flow through a plane that is compatible with the one-dimensional approach of the models proposed previously. Consequently, the heat flow into the ground can be characterized by analyzing the variation of the temperature profile of the soil as a function of the depth. With this experimental information, empirical monitoring of the heat flow and, by repercussion, of the temperature contrast of a buried mine can be performed by evaluating the derivative (or gradient) of the soil temperature as a function of depth. To retrieve this information with sufficient accuracy, the analytical solution of the one-dimensional differential heat equation (eq. 5) is fitted with the experimental temperature readings. Figure 5 shows temperature profiles in a packed gravel road for different times of day with their corresponding numerical fits obtained by using the two first terms of eq. 5.

However, with this approach, one question arises: At which depth should we measure the temperature gradient ? Following the analysis of the simple model, the temperature gradient should be measured at the interface soil-atmosphere to monitor the heat flow on that location. On the other hand, because of the general experimental difficulties associated with the measurement of the temperature on the soil surface, the evaluation of the tempera-

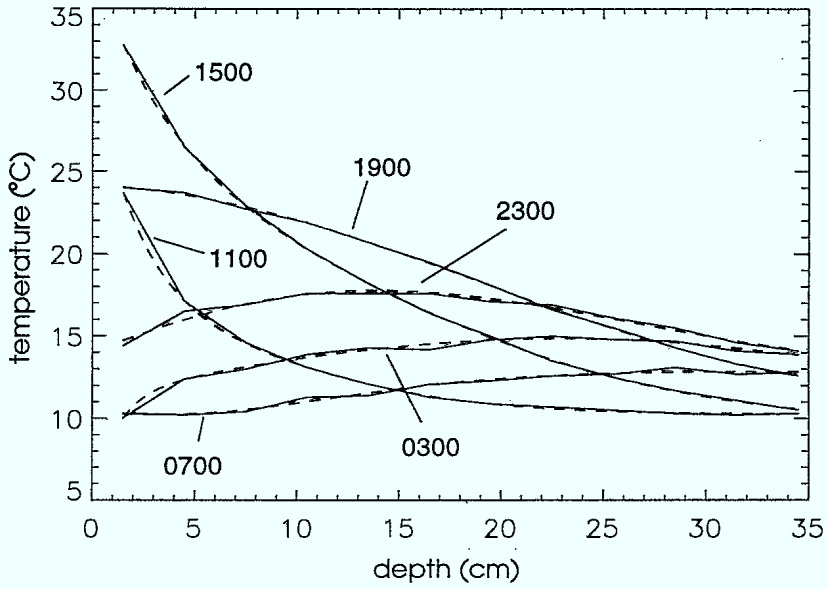

FIGURE 5 – Plot of the temperature profiles with depth in the soil at different times of day. The continuous lines have been obtained by joining 12 temperature readings sampled at 3 cm intervals and the dashed lines are derived from the numerical fittings of the exact solution to the heat equation (eq. 5) with these sampled temperatures. The experimental instrument used to obtain this information is the temperature probe described in Section 3.2.

ture gradient on that location from the fitted analytical solution will imply an extrapolation of the experimentally acquired temperature readings. This could introduce instabilities in the characterization of the heat flow. A method for bypassing this difficulty is to measure the temperature gradient in an interpolation region of the fitted curve. This approach has the advantages of being more stable and accurate and is compatible with the relation proposed by the simple model because of the intrinsic relation between the heat flows at different depths. On the other hand, the depth at which the gradient is measured should not be too deep because of the time period associated with the distributed heat capacitance of the soil column. An adequate choice for the depth at which the temperature gradient is measured should be dictated by the anticipated average depths of the buried mines. For

these reasons, we arbitrary chose to evaluate the temperature gradient in the soil at a depth of 7 cm for all the experimental results shown in Chapter 4.0.

3.0 DESCRIPTION OF THE EXPERIMENTAL INSTRUMENTATION

The work reported in this document aims at answering two main questions: How efficient is the passive IR imaging technique to detect low-metal buried landmines under different environmental conditions (especially in the scenario defined by the ILDC program) and are the models described in Chapter 2.0 adequate to identify the optimum and poor detection periods when using that technique ? To answer these two questions, a series of trials have been performed. Carrying out these trials requires different experimental instruments. The present chapter describes this instrumentation. First, the technical specifications of the three thermal imagers used during these trials are shown. Then, the vehicle used for the dynamic trials and the positioning of the thermal imagers on this vehicle are discussed. Finally, the temperature probe necessary for the characterization of the thermal gradient in the soil is detailed.

3.1 Description of the LWIR and MWIR Cameras

Three models of thermal imagers have been used to perform the different trials. At the beginning of the ILDC program, a relatively old model of LWIR imager (the THV-782) has been used for the early tests of the technology. Then, based on these early testings, another model (the THV-1000) was purchased especially for the ILDC program. Most experimental results reported have been obtained with this last thermal camera. Finally, two MWIR imagers (IR-M500 and IR-M600) have been borrowed from a distributor for comparison purposes. These cameras are described in the next three sections.

3.1.1 The THV-782 LWIR Camera

At an early stage of the investigation of the detection of buried landmines by thermal imaging, few trials were performed with a relatively old model of LWIR camera. Although its limited data acquisition capabilities, this camera was useful for the early investigation work of the ILDC program. Table I shows the technical specifications of this camera.

TABLE I

Technical specifications for the THV-782 LWIR camera

Characteristics	**Specifications**
Manufacturer	Agema Infrared Systems
Model	THV-782
Detector	HgCdTe single photoconductive element
Spectral range	8-12 μm
Cooling	LN2
Field of view (HxV)	20^o x 20^o
Temperature range	-20°C to 1000°C
Field frequency	25 Hz
Line frequency	2500 Hz
Lines per frame	280 (interlace 4:1)
Resolving power	100 elements/line
Sensitivity	0.1°C at 30°C
Operating temperature	-15°C to 55°C
Weight	1.6 Kg
Output	RS-170 electronic interface

3.1.2 The THV-1000 LWIR Camera

This camera has been chosen at the beginning of Phase I of the ILDC program. This choice was based on the assumption that thermal measurements in open space are best

taken in the LWIR spectral band [5]. Once the spectral band is chosen, the final choice for the model of camera was based on six criteria: commercial availability, compactness, ruggedness, high spatial resolution, temperature resolution (NETD) smaller than .2°C, and a sufficiently wide field of view to cover easily a width of 3 m to satisfy the design restrictions of the ILDC program. After evaluating the possible models and manufacturers, it has been found that the THV-1000 from AGEMA Infrared Systems was the most suitable for the project. In addition to satisfying the basic criteria identified, this camera has the advantage of possessing a fast 12-bits digital output (SBUS interface) and a serial communication link for remote configuration changes. The digital output feature opens the possibility of accessing the full spatial resolution of the camera and of extracting image frames with complete thermal information. The relation to convert the pixel readings (pix) to its corresponding temperature (T) was evaluated in laboratory with a black body reference for temperatures ranging between -10°C and 50°C as a parabolic equation. This equation has been derived as:

$$\mathrm{T} = -7.600 \times 10^{-06} \times (pix)^2 + 0.06629 \times (pix) - 53.02. \qquad [7]$$

The access to IR images containing the complete thermal information makes it possible, with the serial communication link, to modify the configuration of the video output (view by the ILDC operator) as a function of the thermal characteristics derived from the 12-bits digital extracted images. This digital output capability was also widely used during the static and dynamic trials. Table II shows the main specifications associated with this camera.

[5] This assumption has been confirmed by comparing directly the experimental results obtained with an MWIR and an LWIR camera (see Section 4.4).

TABLE II

Technical specifications of the THV-1000 LWIR camera

Characteristics	**Specifications**
Manufacturer	Agema Infrared Systems
Model	THV-1000
Serial number	114103
Detector	Five-element SPRITE
Spectral range	8-12 μm
Cooling	Integral Stirling cooler
Field of view (HxV)	62.5° x 41.5°
Instantaneous FOV	1.88 mrad
MRTD typical	0.5°C (at 0.26 cycles/mrad) 0.08°C (at 0.13 cycles/mrad)
NETD	0.18°C
Dynamic range	12 bits
Samples/line	800
Active IR-lines (EIA/CCIR)	400/450
Frame frequency	30/25 Hz
Video output	S Video, RGB, NTSC
Digital output	Taxi to SBUS Interface
Serial communication	RS422 and RS232
MTBF	5500 hrs
Power	20-35 V DC, max. 60 W
Operating temperature	-15°C to 55°C
Storage temperature	-40°C to 70°C
Dimension	307x159x202 (mm^3)
Shock/vibration	25 G/2 G IEC 68
EMI	US.FCC and IEC 801
Safety standard	IEC 950
Weight	~6 kg

3.1.3 The IR-M500 and IR-M600 MWIR Cameras

Two MWIR cameras have also been tested under the ILDC program. These cameras have the advantage of being based on focal plane array (FPA) technology. This configuration eliminates all moving parts, except for the cooling system which is, as the THV-1000, an integral Stirling cooler. The FPA technology improves the ruggedness and the image stability of the camera, which are appealing for the ILDC program. However, as reported in Section 4.4, there are other aspects intrinsically associated with the conditions of operation of thermal detection technology for ILDC which disadvantage MWIR based thermal cameras. Nevertheless, two models of MWIR cameras, the IR-M500 and the IR-M600 (the latter having a better filling ratio), based on the platinum-silicide technology and made by Mitsubishi Electronic Corporation, have been used to gather the information shown in the next chapter. Table III reports the technical specifications of these cameras, as provided by the manufacturer.

3.2 The Temperature Probe

The models developed in Chapter 2.0 introduce the possibility of characterizing the level of temperature contrast of a buried mine site by evaluating the temperature gradient in the soil. To obtain this information during the different trials, a temperature probe has been developed in house. This temperature probe is built with a plexiglas tube (1" in diameter) along with 15 thermocouples of type T which were fixed 3 cm apart. The acquisition of the temperature was done manually with a calibrated thermocouple reader or automatically with the help of a computer. The computerized acquisition was done with an analog-to-digital conversion board (Model DT2837, S/N 00307550) and a screw terminal board (DT717-T) from Data Translation Inc. The resulting temperature (T) associated

TABLE III

Technical specifications of the IR-M500 and IR-M600 MWIR cameras

Characteristics	**Specifications**
Manufacturer	Mitsubishi Electronic Corporation
Model	IR-M500 [IR-M600]
Detector	Platinum Silicide Schottky-Barrier IRSCD
Array size	512x512 pixels
Spectral range	3-5 μm
Field of view (HxV)	28^o x 22^o (25 mm lens)
NETD	0.15 [< .1] ^{o}C
Field time	1/60 sec
Cooling	Integral Stirling cooler
Image display	Monochromatic, 256 levels of grey
Video output	RS-170
Digital output	RS-422 (10 bit, 9.2 MHz)
MTBF	4000 hrs
Power	22-28 V, 150 W
Operating temperature	-10^{o}C to 50^{o}C (humidity less than 95 %)
Weight	$\sim$8 kg
Dimension	136x390x153 (mm^3)

Notes: The specifications of the IR-M600, when different from the ones provided for the IR-M500, are in square brackets.

with each thermocouple is obtained by using the voltage conversion equation for the T thermocouple found in the OMEGA temperature Handbook (Ref. 14) given as:

$$\mathrm{T} = a_0 + a_1 \times vc + a_2 \times vc^2 + a_3 \times vc^3 + a_4 \times vc^4 + a_5 \times vc^5 + a_6 \times vc^6 + a_7 \times vc^7 \quad [8]$$

where a_n is the n fitting coefficients given as

coefficients	values	coefficients	values
a_0	0.10086091	a_4	-9247486589
a_1	25727.94369	a_5	6.97688×10^{11}
a_2	-767345.8295	a_6	-2.66192×10^{13}
a_3	78025595.81	a_7	2.94078×10^{14}

and where vc is the corrected voltage reading evaluated as

$$vc = vs + ve. \quad [9]$$

In this last equation, vs and ve are the differential voltage (v) associated with the thermocouple and the corrected voltage factor resulting from the cold junction, respectively. The conversion from the digital readings ($step$) provided by the A/D board to v is done with the following equation:

$$v = (\frac{step}{65536} \times 20 - 10)/500. \quad [10]$$

This relation is derived from the board configuration which was: 16-bits conversion, bipolar readings (-10 volts to 10 volts), and a 500 gain factor. On the other hand, the correction

factor (ve) is obtained in two steps. First, the differential voltage of the cold junction is evaluated by converting the digital reading of the acquisition board to its equivalent voltage ($\bar{ve}$) using eq. 10. Then, a temperature correction factor (tc) is derived from the equation provided by the manufacturer of the temperature acquisition board (DT717-T) (Ref. 15). This equation is

FIGURE 6 – Picture of the temperature probe

$$tc = \bar{ve} \times 1000/0.5 \qquad [11]$$

Finally, the equivalent corrected voltage factor associated with the cold junction (ve) is evaluated by inverting eq. 8 with the temperature correction factor (tc).

ILDC Notes: As mentioned previously, the temperature probe described is used for the evaluation of the temperature gradient and may become a useful tool to predict the temperature contrasts of buried mines. In the case where this technique becomes clearly useful for the ILDC program, it is assumed that the involvement of a company like Geotherm Inc., with his accumulated expertise in the thermal characterization of soils, should be valuable for the design of robust temperature probes and possibly for the processing of the temperature readings.

3.3 The Trial Vehicle

In Chapter 4.0, a series of experimental results are given for trials in which the IR camera is moving. These dynamic trials, which are designed to simulate different aspects of the demining scenario defined by ILDC, are performed with a ground vehicle. For the trials performed in Alberta, the ground vehicle has the capability to record visible and IR video. Also, this vehicle has an integrated Sun station which makes it possible to record digital images output by the THV-1000 LWIR camera through the SBUS interface. To facilitate digital image acquisition, this vehicle is also equipped with a fifth wheel in order to measure precisely the distance travelled during the trials. A similar vehicle is used for the trials performed in Eastern Canada. With either vehicle, the IR camera is placed on a support directly in front of the vehicle at an approximative height of 3 m with about 45^o incline. With this configuration, the FOV of the camera covers an area of 4 m in width at the bottom of the frame and 8 m in width at the top of the frame with 5 m in depth. In addition, this area is beginning at less than 1.5 m in front of the vehicle. Especially during the dynamic trials performed at Wainwright (see Subsection 4.2.2), an on-board audio communication system, which may be recorded on videotape with the IR and visible

images, allows communication between the back and the front of the vehicle. Finally, speed as low as 2.5 km/hr was reachable with the vehicle used in the Alberta trials.

FIGURE 7 – Picture of the trial vehicle

3.4 The Polymeric Material Used to Simulate TNT

For most trials, a large fraction of IR surrogates is used instead of real mines. This substitution has the advantage of reducing considerably the safety procedures associated with the manipulation of explosives. To achieve this substitution while keeping the thermal characteristics of these surrogates comparable to real mines, an urethane rubber is used as a filling compound or is directly cast to obtain the equivalent thermal mass of the replicated mines. The urethane rubber used for all replica mines is the "Adiprene L-100" made by

Uniroyal. This choice is based on the value associated with the heat conductivity of this rubber, evaluated by the manufacturer to 0.132 W/(m-^{o}C), which is equivalent within 10 % to the heat conductivity of TNT, itself evaluated by Patel (Ref. 12) to 0.146 W/(m-^{o}C). The level of validity in the choice of this compound reproducing the thermal characteristics of real buried mine sites has been proven legitimate experimentally (see paragraph entitled "The validity of the IR signature associated with the developed mine surrogates" on page 73).

4.0 TRIAL DESCRIPTIONS AND EXPERIMENTAL RESULTS

In this chapter, the results of a series of trials aiming at validating experimentally the proposed models, and more important, at evaluating the capability of IR technology to detect buried landmines are reported. First, the fundamental aspects of the buried mine IR signatures as their apparent temperature contrast amplitude and variability with external parameters are evaluated in static trials. Then, the practicability of this technology for the ILDC program is especially investigated. For that purpose, special care is taken to simulate as close as possible the scenario addressed by the ILDC project. Finally, the results of a series of secondary trials that were performed to answer important aspects of the use of IR technology in the ILDC project are discussed.

4.1 Static Trials

The trials reported in this section have been carried out to evaluate the basic thermal characteristics of the buried mine IR signature. Features as temperature contrast variations during a 24-hour cycle and with the depth of the buried mine are especially investigated. To obtain this information, IR mine surrogates are buried at known depths on packed gravel roads and the THV-1000 LWIR camera is positioned on a set location with an adequate FOV over the buried mine sites for the full periods of the two main static trials. To evaluate the variability of these basic thermal characteristics as a function of the geographical region, a first trial is performed in the Prairies and a second one in the Canadian Shield region (Eastern Canada). Table IV describes the experimental settings of these two trials. Digital images of the buried mine sites are taken at one-hour intervals. Subsequently, the pixel contrast of a buried mine is evaluated in laboratory by subtracting the pixel-averaged value of a small square area at the centre of the blob created by the buried

mine and the pixel-averaged value of a representative reference square surface close to the buried mine. Then, the calibration curve given by eq. 7 is introduced to convert the pixel contrast into an apparent temperature contrast. In parallel with digital image acquisition, the temperature variations of the soil with depth are also collected with the temperature probe. This temperature profile is acquired manually with a thermocouple reader at the same time intervals as the digital image acquisition. Later, in laboratory, the temperature gradients are derived from these temperature profiles, as described in Section 2.4. The experimental results of the trials performed in the Prairies and the Canadian Shield region are shown below in two formats. First, the thermal variables, the temperature contrasts of the buried mines and the temperature gradients in the soil, are plotted as a function of time (Figs. 8 and 9). These graphs display well the four different states of the heat exchanges between the atmosphere and the soil: the morning (MT) and evening (ET) transitions periods during which the temperature contrasts of the buried mines disappear, the optimum day (OD) and night (ON) periods during which the temperature contrasts of the buried mines are maximum (positively or negatively). Second, the temperature contrasts of the buried mines is plotted as a function of the temperature gradients in the soil (Figs. 10, 11 and 12). These correlation plots reveal many important features [6] enhancing the comprehension of the IR signature of a buried mine. They are:

- The relation between the temperature contrasts of the buried mines and the temperature gradients in the soil is closely linear, as predicted by the models presented in Section 2.1.

- When a straight line is least square fitted with the points of the correlation between the temperature contrasts of the buried mines and the temperature gradients in the soil,

[6] For aesthetic reasons, the temperature gradients are multiplied by -1 to give a positive correlation with the temperature contrasts of the buried mines.

the slope of this straight line increases with the depth of the buried mine decreasing as expected.

- The important standard deviations of the correlated points around the fitted straight line during the positive temperature contrast (daytime) can be associated with sun radiation cluttering.

- The recent buried mine sites showing surface thermal effects (see Chapter 2.0) exhibit more important standard deviations during daytime than the older buried mine sites where only volume thermal effects are present.

- For mines of similar thermal masses, buried in the same type of roads and at equivalent depths, the slopes of their corresponding fitted straight lines are comparable, whether the mines are buried in the Prairies or in the Canadian Shield region.

TABLE IV

Experimental settings of the two static trials reported

	Canadian Prairies trial	**Canadian Shield trial**
Surrogates used	2 replicated AT TMN-46 filled with the plastic simulating TNT	3 AT TMA-3 surrogates and 3 AP PMN-6 surrogates directly cast with the plastic simulating TNT. In addition, two empty refilled holes were made to reproduce the hole thermal effects for the AT and AP mines.
Burying depths	5 and 7 cm	0.5, 2cm and 4 cm
Burying period	8 months before trial	A few days before trial
Trial period	32-hour trial beginning at 8:00, May 10, 1995	48-hour trial beginning at 17:00, June 6, 1995

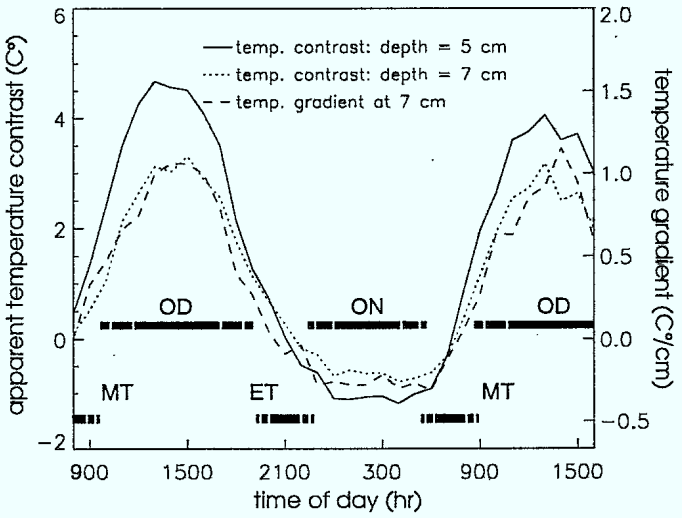

FIGURE 8 – Plot of the temperature contrasts of two buried mines (TMN-46 surrogates) and the measured temperature gradients as a function of time over the 32-hour trial performed in the Canadian Prairies.

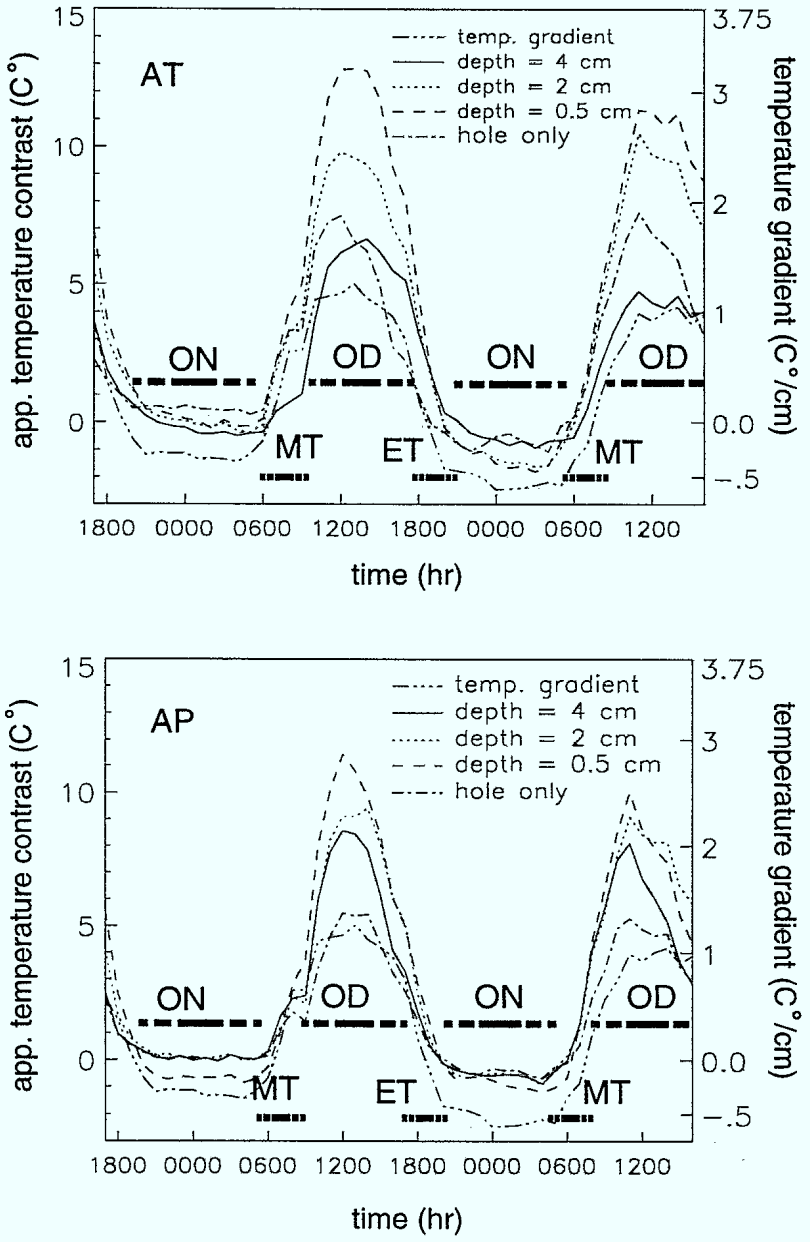

FIGURE 9 – Plots of the temperature contrasts of three buried AT TMA-3 surrogates and a refilled AT size empty hole (AT plot), three buried AP PMN-6 surrogates and a refilled AP size empty hole (AP plot) and the measured temperature gradients at a depth of 7 cm as a function of time over the 48-hour trial performed in the Canadian Shield region.

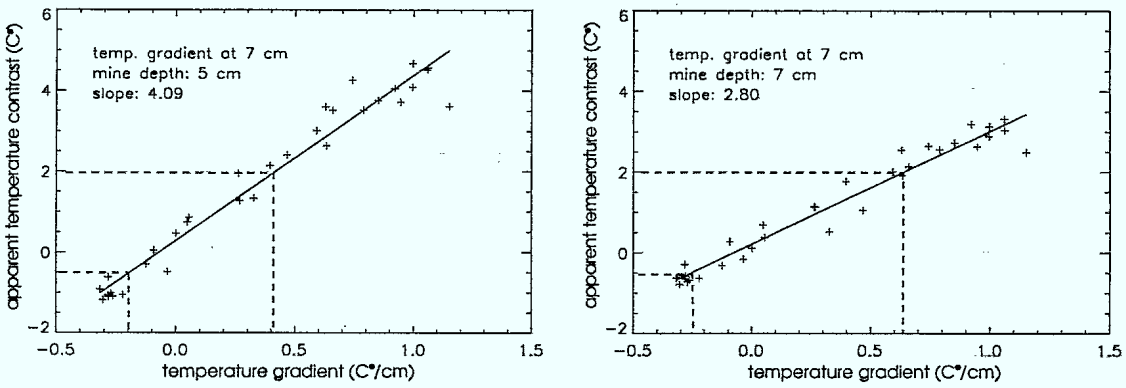

a) b)

FIGURE 10 – Plots of the correlation between the temperature contrasts of the buried mines and the temperature gradients in the soil for the experimental data shown in Fig. 8. The straight lines are obtained from a standard first-order polynomial least square fits through these points.

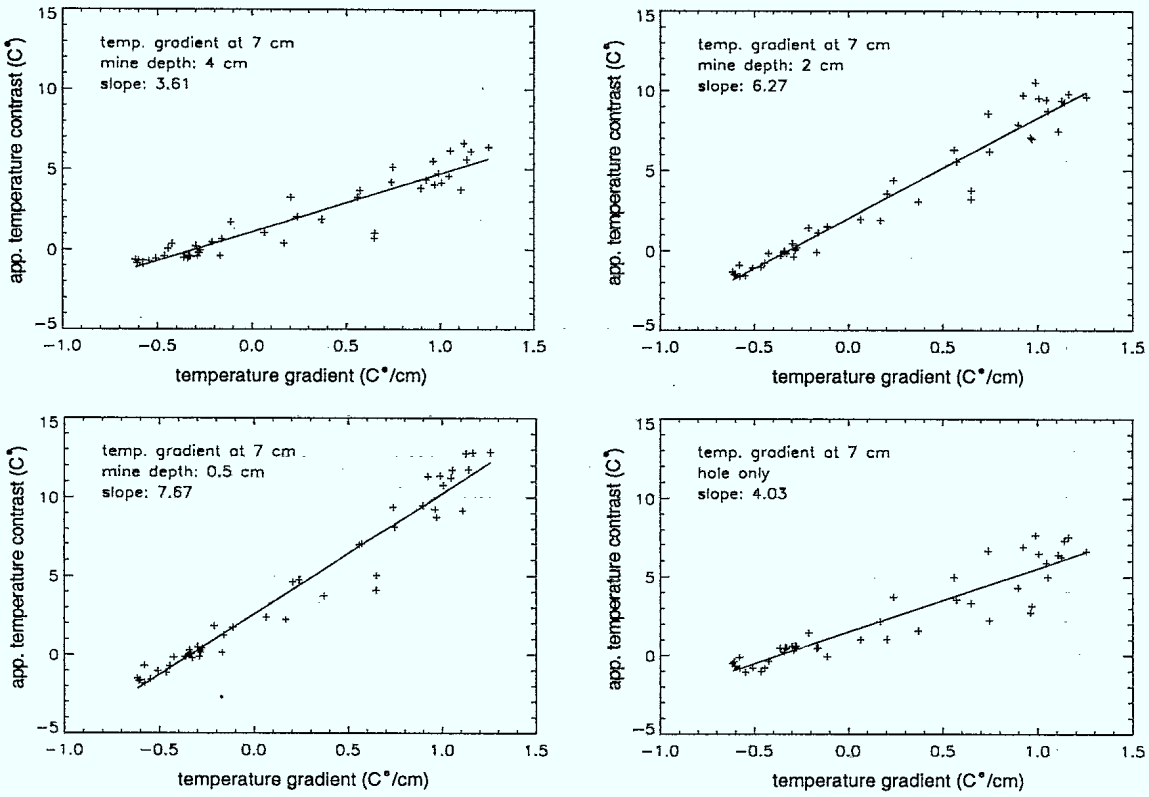

FIGURE 11 – Plots of the correlation between the temperature contrasts of the buried mine surrogates and the temperature gradients in the soil for the experimental data shown in Fig. 9 (AT plot). The straight lines are obtained from a standard first-order polynomial least square fits through these points.

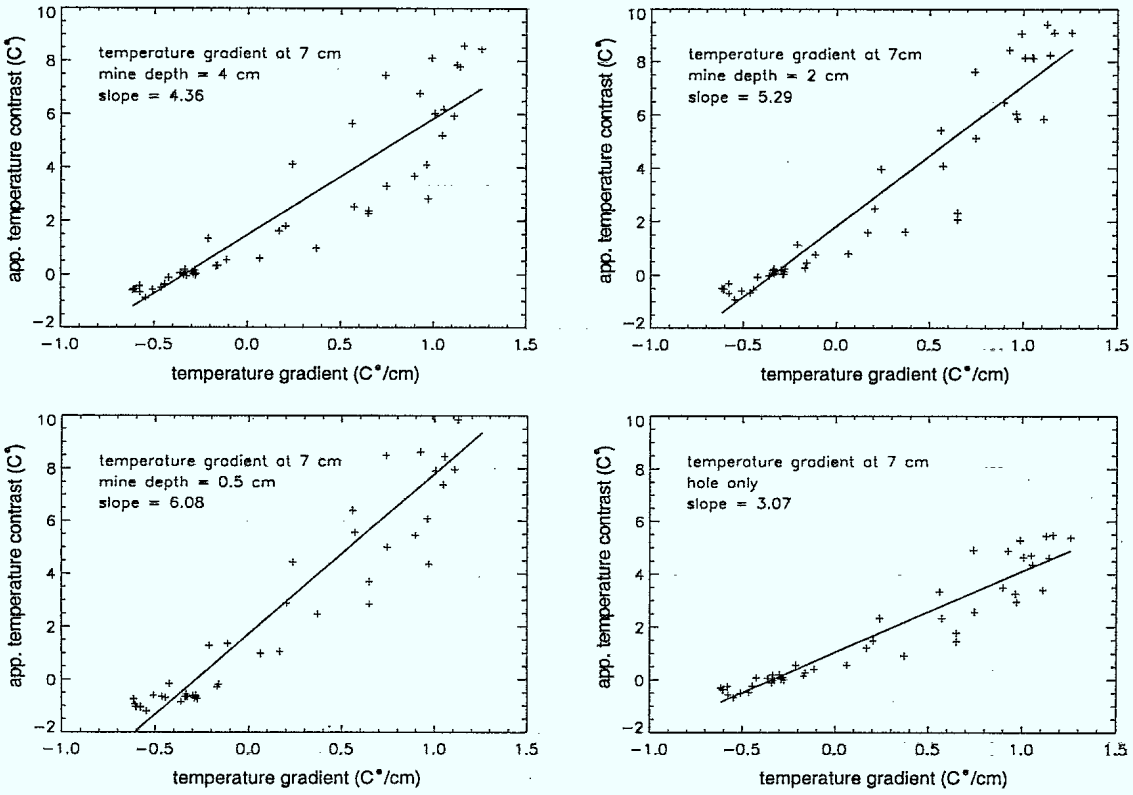

FIGURE 12 – Plots of the correlation between the temperature contrasts of the buried mine surrogates and the temperature gradients in the soil for the experimental data shown in Fig. 9 (AP plot). The straight lines are obtained from a standard first-order polynomial least square fits through these points.

4.2 Dynamic Trials

In the previous section, basic information on the characteristics of the formation of the buried mine IR signatures are reported as: the expected amplitude of the apparent temperature contrast and the variability of this contrast with time of day, depth of the mine, and geographic location. In addition, experimental results used to verify the validity of the models proposed in Chapter 2.0 are also reported. In this section, practical answers to the applicability of IR technology in the ILDC program are sought. For that reason, most trials reported are performed with the IR camera in movement and a human operator. These trials are carried out on two different sites: the "Radar Road" trial site at Canadian Forces Base Suffield (CFB Suffield) and at CFB Wainwright. On the first trial site ("Radar Road"), the apparent temperature contrast threshold necessary for a human operator to detect a buried mine site by IR video inspection is evaluated. Also on that site, the behaviour of the IR detection technology in a winterlike environment is investigated. On the second site (CFB Wainwright), an important trial is performed to evaluate the capacity of IR technology to detect low-metal buried mines in a scenario as close as possible to the one addressed by the ILDC program. For that purpose, the technology is tested on a packed gravel and a sand road about 5 km long with real mines. From that trial, realistic values for the IR detection efficiencies and the false alarm rates are reported.

4.2.1 The "Radar Road" Trial

The trials described in the next two sections were performed on a packed gravel road located at CFB Suffield. This site , referred to as "Radar Road", was built to obtain a basic characterization of IR technology for the detection of low-metal buried mines. A section of that road (see Fig. 13), 200 m long, where 20 AT TMA-3 and 40 AP PNM-

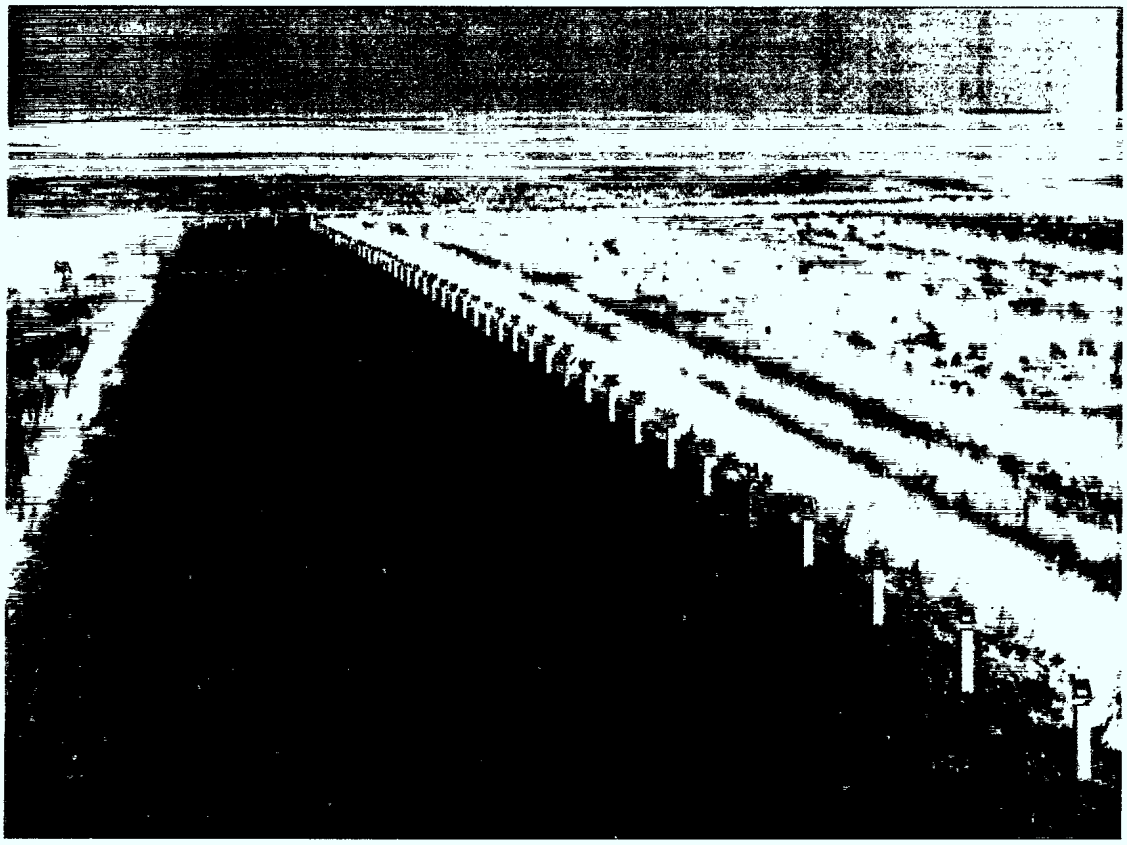

FIGURE 13 – Picture of the "Radar Road" trial site with the surrogates at the surface.

6 surrogates were buried at depths of less than 7 cm and on well-defined locations (see Table V and Fig. 14 for the specific descriptions of the locations of these surrogates), was chosen. To facilitate the analysis of the IR images obtained in the different trials performed on the Radar Road site, a series of posts located on the side of the road provide a spatial reference system allowing the identification of each mine site by monitoring directly the IR videotapes recorded. These surrogates were buried on December 1st, 1994. During the burying operation, because of the frozen state of the road, important surface textures were created on each burying site, which left important thermal surface effects easily observable with the IR camera. This aspect has created difficulties in the evaluation of the detection

efficiency of the technique and will be mentioned further in the description of the winter trial.

Human IR Detection Threshold Measurements

This section reports a trial to evaluate the apparent temperature contrast thresholds of buried mine IR signatures in order to allow its detection with IR technology. For that trial, the detection threshold is based only on the temperature contrast of the buried mine which is at its best incomplete. A more exhaustive approach should include many other variables like the size and shape of the IR blobs, the level of clutter, and if the detection has to be performed by video inspection, the effectiveness factors of the human operator. A complete characterization of all these variables in the evaluation of the detection threshold is quite difficult and would necessitate much more controlled trials than the one reported in this section. However, efforts have been deployed to take into account some of these variables by establishing different apparent temperature contrast thresholds for AT and AP mines, and for the day and night periods. The apparent temperature contrast plots in Figs. 15, 16, 17 and 18 were gathered with the THV-1000 LWIR camera. These contrasts are obtained by following the same procedure as the one described in Section 4.1 with, this time, the digital images acquired at given travel distance intervals, while driving over the "Radar Road" site with the trial vehicle. The evaluation of the apparent temperature contrast thresholds are performed in two steps. First, the AT and AP buried mine sites are classified as detected or not by visual inspection of the videotapes recorded with the IR camera during the different passes. During that procedure, to limit the effects of knowing where the mines are buried, special care is taken to identify only clearly observable IR signatures as detected buried mine sites. From this visual classification and the digital information, an apparent temperature contrast threshold is derived by identifying the levels of contrast separating the detected

TABLE V

Spatial positions of the AT and AP surrogates on the "Radar Road" trial site

# AT surrogate	# post	distance (m)	configuration	depth (cm)
1	1	1.80	A	T3.5, 1P1, 2P0.5
2	4	3.20	B	T4, 1P0.5, 2P1.5
3	6	1.80	C	T4, 1P0.5, 2P1
4	9	3.20	D	T4.5, 1P2, 2P3.5
5	11	1.80	E	T1, 1P3, 2P1
**	12	3.0	F	hole only
6	14	3.20	F	T2.5, 1P2.5, 2P1
7	16	1.80	A	T2, 1P1.5, 2P1
8	19	3.20	B	T5, 1P0.5, 2P2
9	21	1.80	C	T5.5, 1P2, 2P2.5
10	24	3.20	D	T2, 1P1, 2P1.5
11	26	1.80	A	T1.5, 1P0.5, 2P0.5
**	28	2.0	C	hole only
12	29	3.20	F	T4, 1P1, 2P0.5
13	31	1.80	A	T1, 1P1.5, 2P1
14	34	3.20	B	T3, 1P1, 2P1.5
15	36	1.80	C	T1.5, 1P0.5, 2P1
16	39	3.20	D	T1.5, 1P2, 2P0.5
17	41	1.80	D	T3, 1P1, 2P1
**	43	2.0	B	hole only
18	44	3.20	F	T2, 1P0.5, 2P1.5
19	46	1.80	C	T6.5, 1P1.5, 2P0.5
20	49	3.20	B	T3.5, 1P1, 2P2

Notes: For each AT surrogate, the position of the burying site is measured laterally in metres from the specified numbered post. A 4-metre distance separates each post along the 200-meter section of the road. The letters in the configuration column refer to the six possible dispositions of the two AP surrogates buried close the AT surrogates (see Fig. 14). Finally, the depth at which each surrogate is buried is given in the last column: the letters T and P identify the AT and AP surrogates, the numbers 1 and 2 preceding the letter P identify the two AP surrogates in reference with Fig. 14, and the last numbers give the depths of the identified surrogates in centimetres.

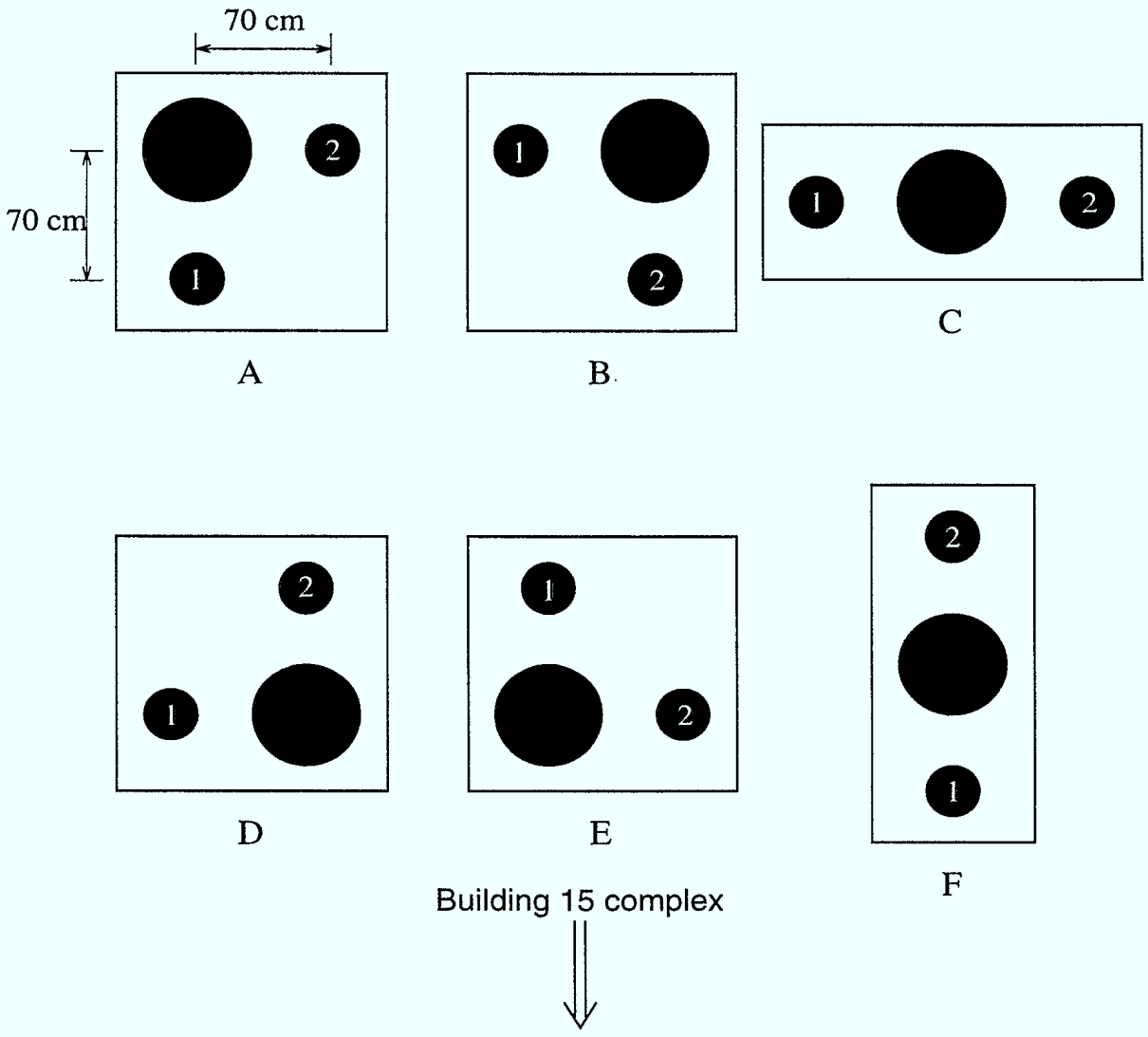

FIGURE 14 – Drawings giving the six spatial configurations of the buried AT and AP surrogates used during the "Radar Road" trials. The large and small black circles represent the AT and AP surrogates, respectively. Each letter identifies a configuration and the numbers 1 and 2 identify specific AP surrogates. These letters and numbers are used as references in Table V. The arrow specifies the orientation of the configurations shown in reference with the direction of the Building 15 complex.

from the undetected buried mines for the different passes. These human-deduced apparent temperature contrast thresholds are given in Table VI.

TABLE VI

Apparent temperature contrast thresholds by human perception

Periods	app. temp. contrast threshold (°C)	
	AT	AP
day	2	2.5
night	0.5	0.6

Notes: These thresholds are approximated by evaluating the minimum apparent temperature contrasts for clearly observable IR signatures of buried mine sites when performing four passes over the "Radar Road" trial site. The detailed apparent temperature contrast distribution of the buried mines used to establish these thresholds are shown in Figs. 15, 16, 17 and 18.

In addition to the acquisition of the IR images with the THV-1000 camera, temperature profiles of the soil are manually sampled before each pass [7]. With these sampled temperature profiles, fits are derived using the method described in Section 2.4 and temperature gradients at a depth of 7 cm are deduced. These thermal characterizations of the soil are shown for each pass at the top of Figs. 15, 16, 17 and 18. From these figures, four important conclusions are deduced:

- The relative apparent temperature contrast variations between buried mine sites when comparing the results of different passes can be related to two possible causes: the error involved in the measure of the apparent temperature contrast due to human interpretations and (or) the inhomogeneity of the local thermal characteristics which can vary with time (as the variation in moisture density).

- Figures 16 and 18 show the occurrence of a weak correlation between the temperature

[7] The temperature probe is positioned on the "Radar Road" trial site at the beginning of the road section.

gradients in the soil and the averaged apparent temperature contrasts of the buried mines. Beside possible experimental errors, these plots reveal a limit of applicability of the predicting property of the temperature gradient. This can be related to the imprecision of the measure or to a weakness of the proposed empirical model itself.

- Even with the above two remarks, as observed in Section 4.1, a general direct relation is observed between the temperature gradient and the averaged apparent temperature contrast of the buried mine sites.

- Finally, the higher apparent temperature contrast threshold identified during daytime supports the theoretical models described in Chapter 2.0 predicting the increase of inherent thermal noise of the IR images of the road by the sun radiation cluttering.

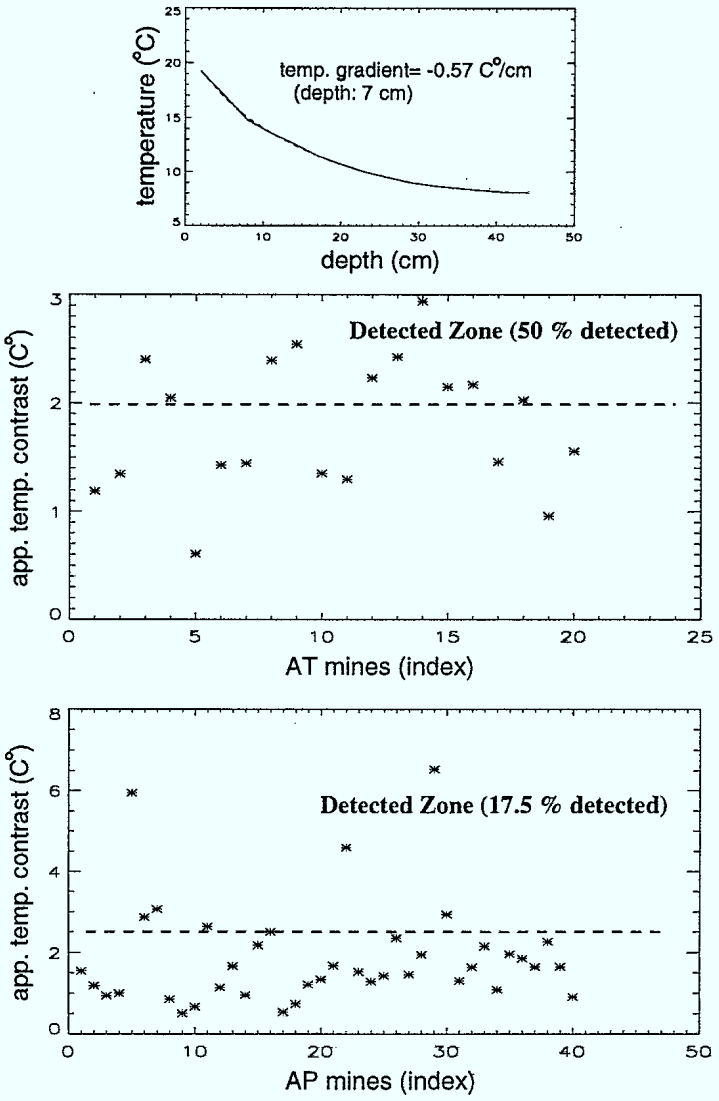

FIGURE 15 – Plots of the thermal characteristics of the dynamic trial performed April 27, 1995 (3:00 PM) at the "Radar Road" trial site. The upper graph shows the acquired (continuous line) and fitted (dashed line) temperature profile of the soil with the corresponding temperature gradient derived at a depth of 7 cm. The two lower graphs show the temperature contrasts of the AT surrogates and the AP surrogates deduced from the digital images acquired during the pass. The dashed lines on these two lower graphs delimit the temperature contrast thresholds for the detection of AP and AT surrogates. These thresholds have been defined by identifying visually the detectable buried mine sites from the videotape and by classifying their corresponding temperature contrasts.

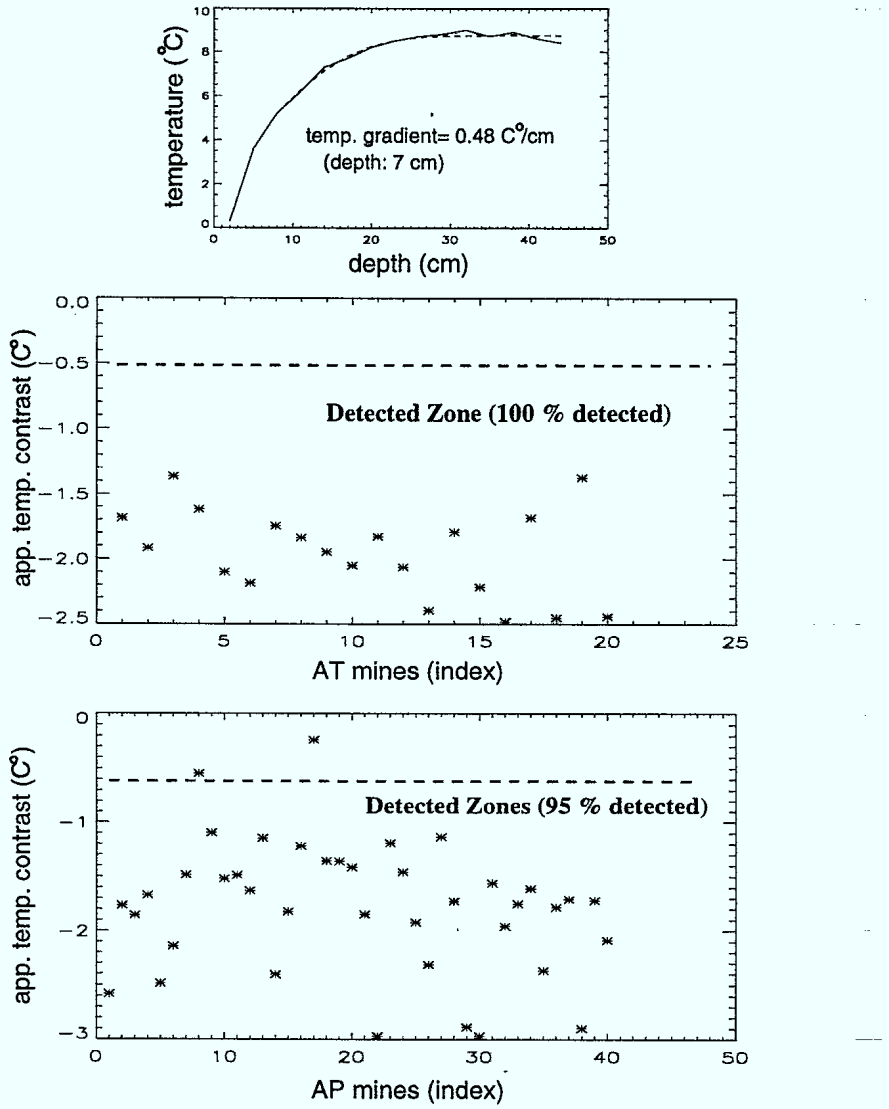

FIGURE 16 – Plots of the thermal characteristics of the dynamic trial performed May 1, 1995 (5:00 AM) at the "Radar Road" trial site. The upper graph shows the acquired (continuous line) and fitted (dashed line) temperature profile of the soil with the corresponding temperature gradient derived at a depth of 7 cm. The two lower graphs show the temperature contrasts of the AT surrogates and the AP surrogates deduced from the digital images acquired during the pass. The dashed lines on these two lower graphs delimit the temperature contrast thresholds for the detection of AP and AT surrogates. These thresholds have been defined by identifying visually the detectable buried mine sites from the videotape and by classifying their corresponding temperature contrasts.

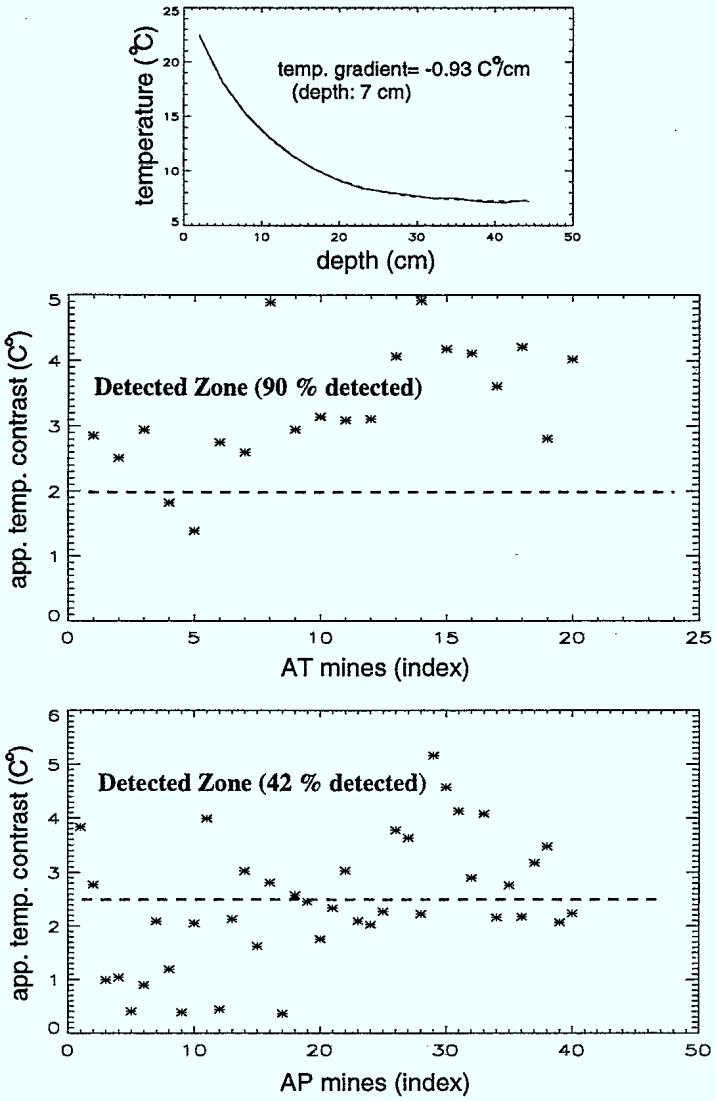

FIGURE 17 – Plots of the thermal characteristics of the dynamic trial performed May 1, 1995 (3:00 PM) at the "Radar Road" trial site. The upper graph shows the acquired (continuous line) and fitted (dashed line) temperature profile of the soil with the corresponding temperature gradient derived at a depth of 7 cm. The two lower graphs show the temperature contrasts of the AT surrogates and the AP surrogates deduced from the digital images acquired during the pass. The dashed lines on these two lower graphs delimit the temperature contrast thresholds for the detection of AP and AT surrogates. These thresholds have been defined by identifying visually the detectable buried mine sites from the videotape and by classifying their corresponding temperature contrasts.

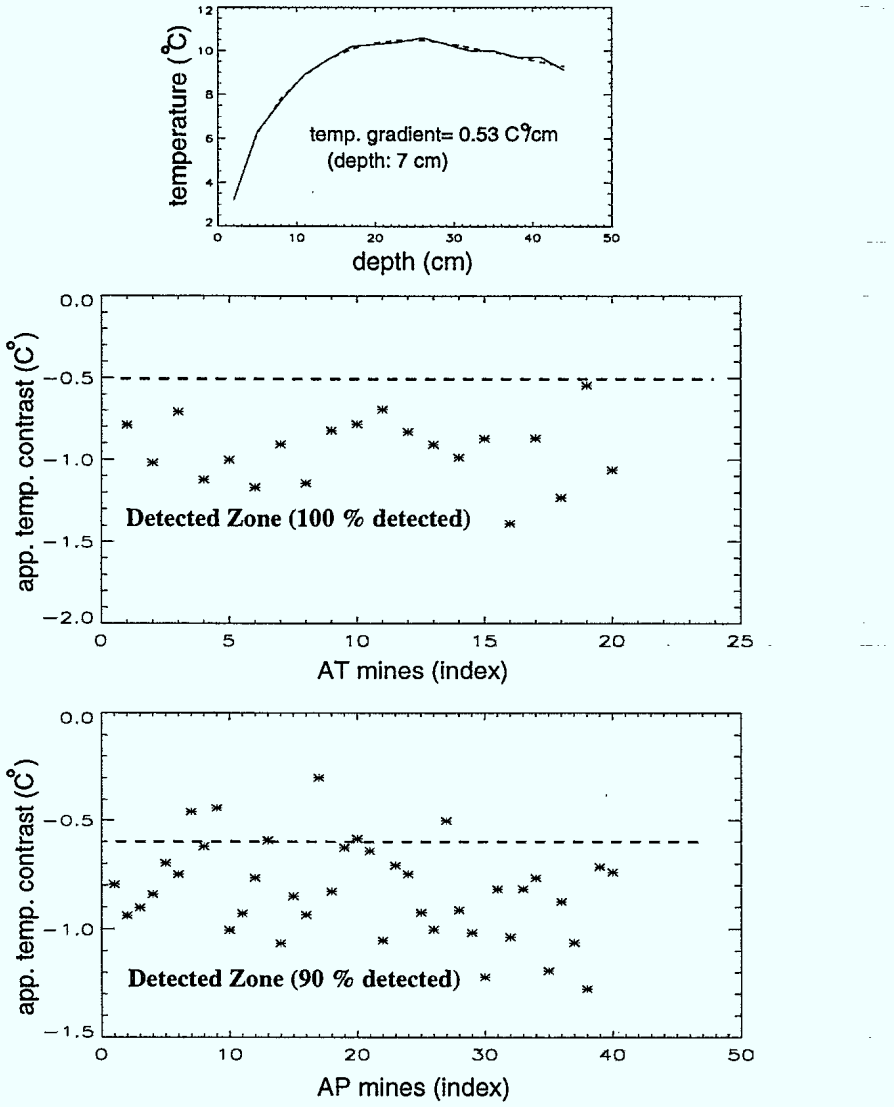

FIGURE 18 – Plots of the thermal characteristics of the dynamic trial performed May 2, 1995 (5:00 AM) at the "Radar Road" trial site. The upper graph shows the acquired (continuous line) and fitted (dashed line) temperature profile of the soil with the corresponding temperature gradient derived at a depth of 7 cm. The two lower graphs show the temperature contrasts of the AT surrogates and the AP surrogates deduced from the digital images acquired during the pass. The dashed lines on these two lower graphs delimit the temperature contrast thresholds for the detection of AP and AT surrogates. These thresholds have been defined by identifying visually the detectable buried mine sites from the videotape and by classifying their corresponding temperature contrasts.

IR Detection under Winterlike Conditions

This section reports one of the earliest trial carried out for the ILDC program. This trial was designed to investigate the efficiency of the IR detection in a winterlike weather environment (trial performed in December 1994 and January 1995). For this work, a second THV-1000 borrowed from Defence Research Establishment Valcartier (DREV) is used. This camera did not have the digital output capability (only video output) and had a lens with a FOV of 20 x 13.3 degrees. Also, because of the early period during which this trial was performed, the temperature gradient characterization technique was not used. This trial is carried out on the "Radar Road" trial site in a way similar to the one described in the previous section. However, the results of the trial are extracted exclusively by a human inspection of the IR video recorded. This method implies that the quantitative results obtained (percentage of detection and false alarm rate) are highly dependent on the human interpretation of what are a detected buried mine site and a false alarm. This is even more delicate when the human analyst knows where the buried mines are. In an effort to reduce the fluctuations associated with the human interpretations, only the IR signatures of buried mines with clearly observable IR contrasts are considered as detected. On the other hand, the level of contrast necessary to identify a false alarm is kept much lower. Nevertheless, even with the serious efforts to follow these two criteria and the fact that the values shown resulted from the averaging over multiple passes, the quantitative values presented should be considered valid only within 10 % for the AT detection efficiency, 20 % for the AP detection efficiency and within 40 % for the false alarm rates (AT or AP). These quantitative results are shown in Figs. 19, 20, 21 and 22 with the atmospheric temperature fluctuations over the month. These temperature fluctuations are obtained from the local weather station. With the purpose of easing the interpretation of these results, the daytime

and night-time trials are shown on different graphs. The encircled numbers in the four figures refer to remarks associated with one specific pass and are given in appendix. These results were the first ones showing in a perceptible manner the improved performance at night with the IR technology. It should also be mentioned that the strong thermal surface effects easily observable during daytime over the buried mines (see the description of the "Radar Road" site in Subsection 4.2.1) for the two months of trial created some dilemma. At first, until December 8^{th}, this effect was not considered as a valid criterion of detection. Then, between December 8^{th} and 19^{th}, even if the IR signatures of the AP mines were not spatially separable from the ones produced by the AT mines (see the spatial distribution of the mines buried on the "Radar Road" trial site in Fig. 14), it was considered that all mines would be detected. Finally, by December 19^{th}, only AP IR signatures that are separable from the ones produced by the AT mines are considered detected.

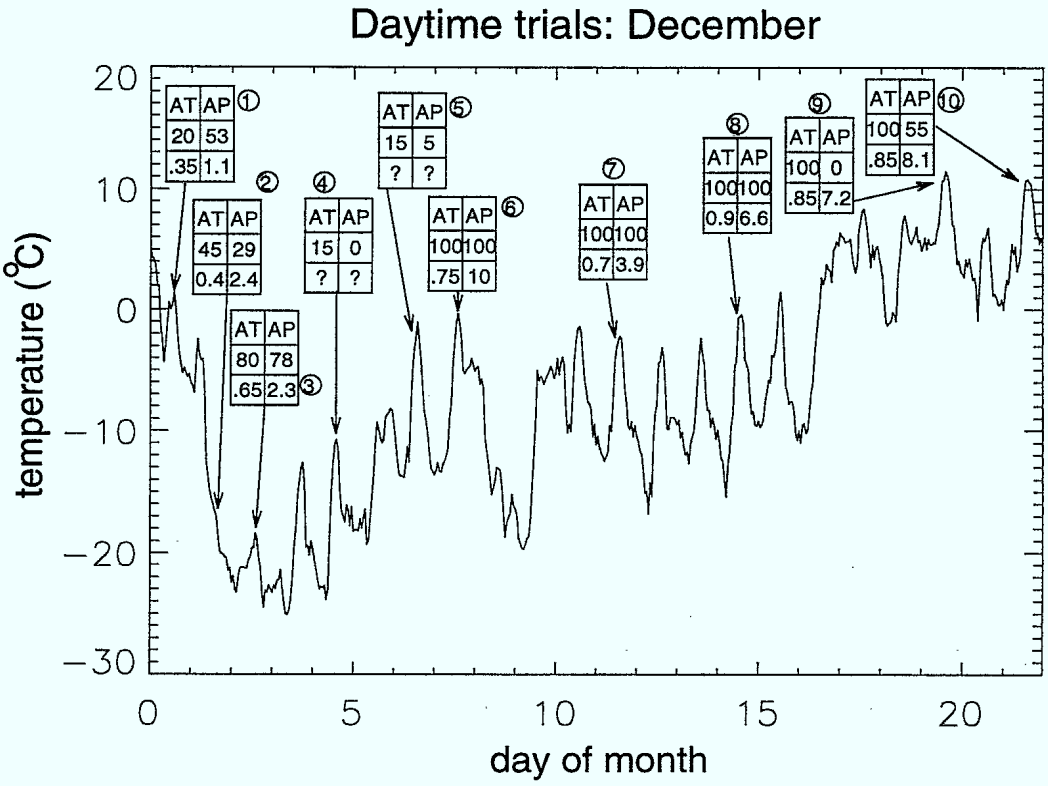

FIGURE 19 – AT and AP detection efficiencies and false alarm rates on the "Radar Road" trial site during daytime with the December temperature evolution. The detection efficiencies (the two upper values) are percentages and the false alarm rates (the two lower values) are per 10 m travelled. The mines buried are TMA-3 and PNM-6 surrogates and the detailed description of the trial is given in the paragraph entitled "IR Detection under Winterlike Conditions" on page 48. The encircled numbers refer to the specific description of the passes given in the enumeration of p. A1.

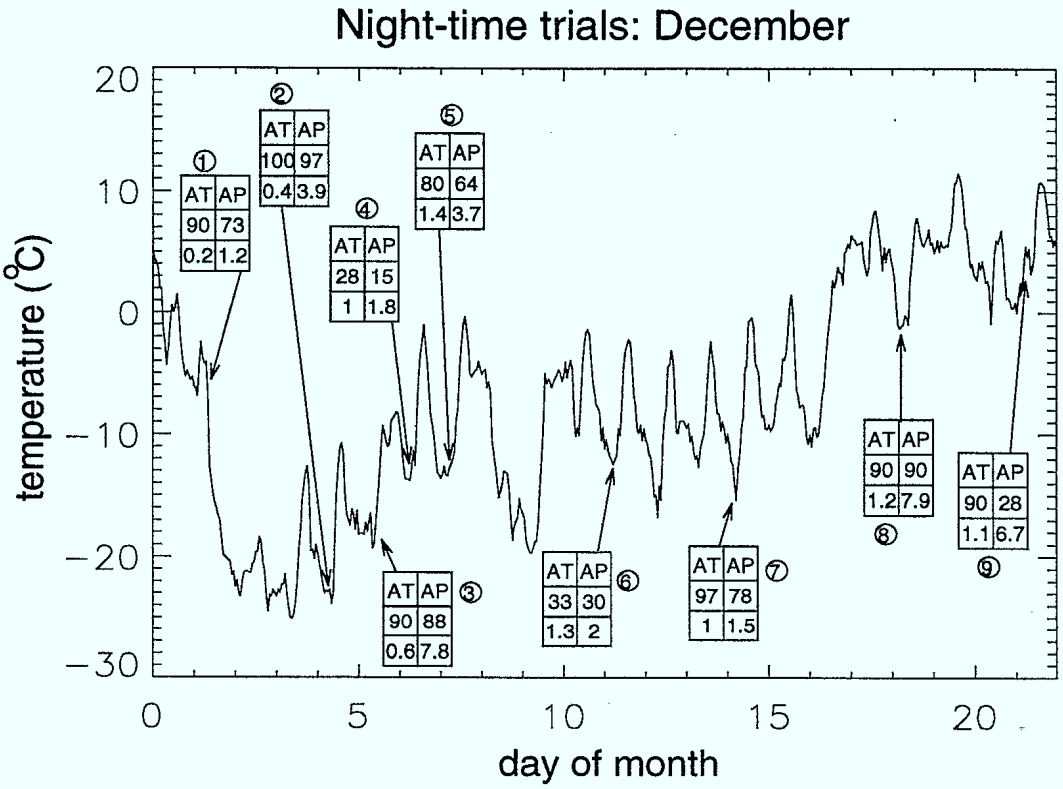

FIGURE 20 – AT and AP detection efficiencies and false alarm rates on the "Radar Road" trial site during night-time with the December temperature evolution. The detection efficiencies (the two upper values) are percentages and the false alarm rates (the two lower values) are per 10 m travelled. The mines buried are TMA-3 and PNM-6 surrogates and the detailed description of the trial is given in the paragraph entitled "IR Detection under Winterlike Conditions" on page 48. The encircled numbers refer to the specific description of the passes given in the enumeration of p. A3.

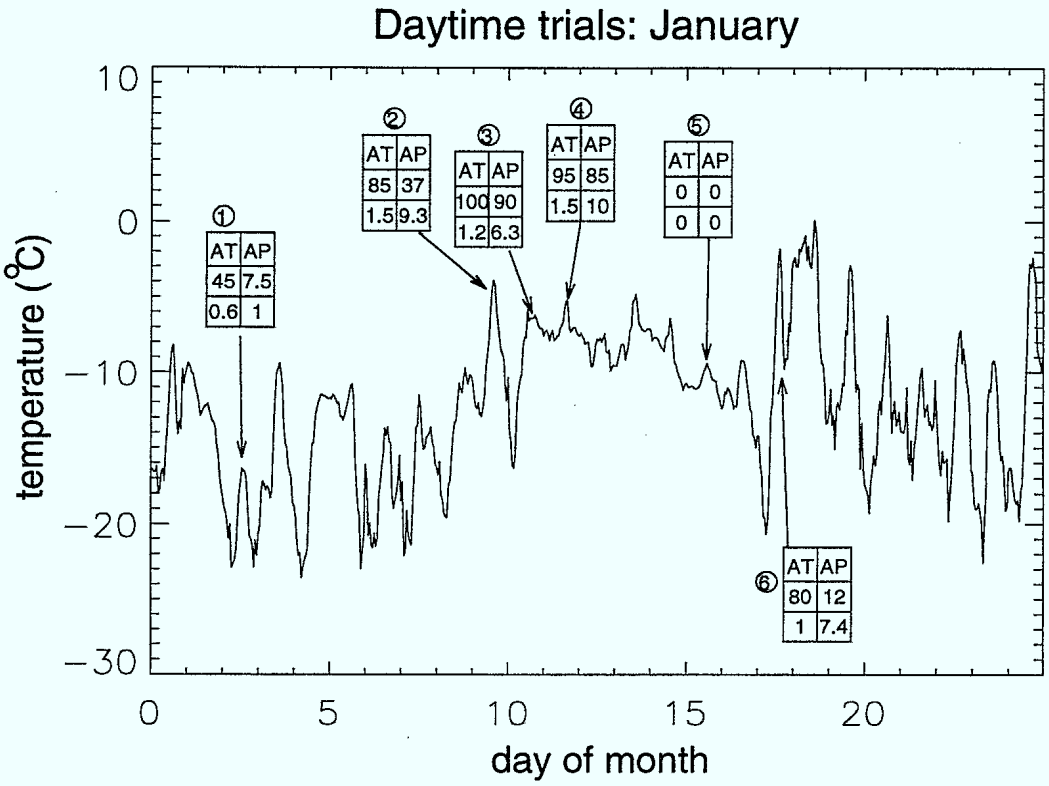

FIGURE 21 – AT and AP detection efficiencies and false alarm rates on the "Radar Road" trial site during daytime with the January temperature evolution. The detection efficiencies (the two upper values) are percentages and the false alarm rates (the two lower values) are per 10 m travelled. The mines buried are TMA-3 and PNM-6 surrogates and the detailed description of the trial is given in the paragraph entitled "IR Detection under Winterlike Conditions" on page 48. The encircled numbers refer to the specific description of the passes given in the enumeration of p. A4.

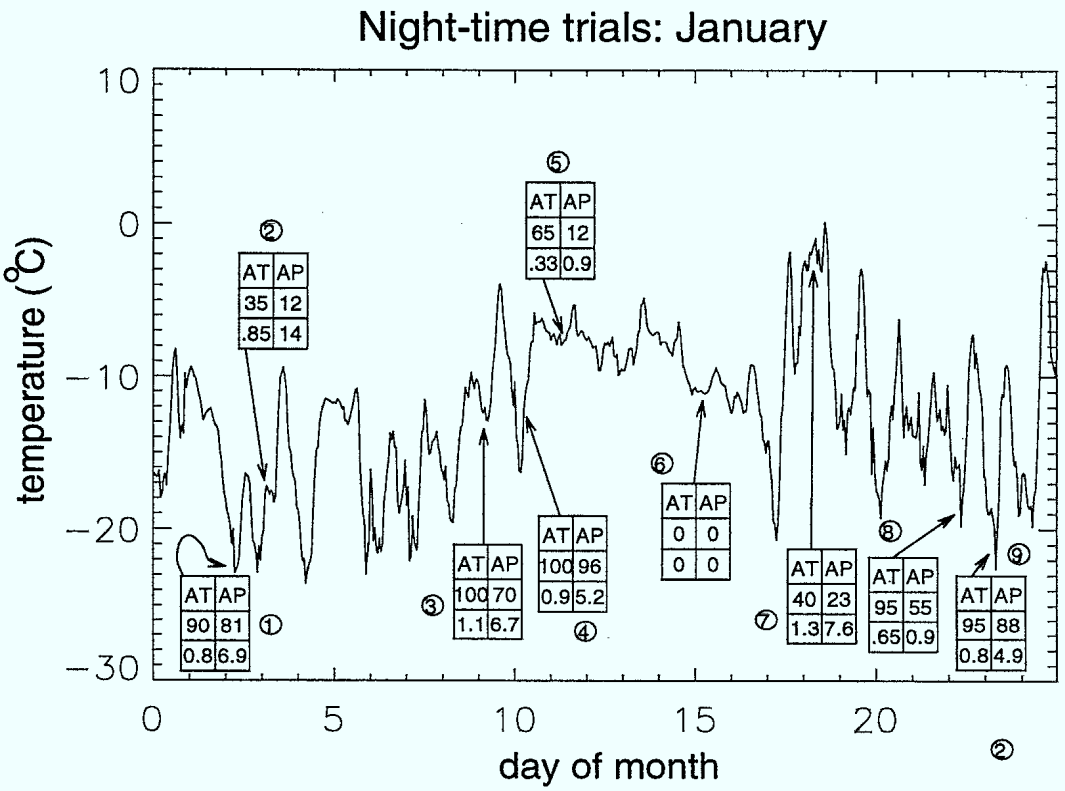

FIGURE 22 – AT and AP detection efficiencies and false alarms rate on the "Radar Road" trial site during night-time with the January temperature evolution. The detection efficiencies (the two upper values) are percentages and the false alarm rates (the two lower values) are per 10 m travelled. The mines buried are TMA-3 and PNM-6 surrogates and the detailed description of the trial is given in the paragraph entitled "IR Detection under Winterlike Conditions" on page 48. The encircled numbers refer to the specific description of the passes given in the enumeration of p. A5.

4.2.2 Wainwright Trial

In order to evaluate the capability of IR technology in the ILDC program, a trial has been independently prepared by the Canadian Forces at DRES. This trial was designed to simulate as closely as possible the demining operations addressed by the ILDC program. With this goal in mind, two road sections were chosen at Canadian Forces Base Wainwright. The first road (see upper picture shown in Fig. 23), intended to reproduce demining operations on a packed gravel road without shadowed area, was approximately 5 km long. The second road (see lower picture shown in Fig. 24), a sand road [8] approximately 4.5 km long with heavy vegetation sections, was chosen to simulate the situations in which a road is partially covered by shadow. The day before the trial, a mixture of different types of real anti-tank mines (TMA-3, Mk-7, M21, VS-2.2), real antipersonnel mines (VS-50, PMA-3) and surrogates were buried randomly along these two roads. The depths at which these mines were buried varied from less than 1 cm for the AP mines to a maximum of 5 cm for the AT mines. Tables VII and VIII describe in detail the spatial distribution of these mines along the packed gravel and the sand roads, respectively.

During the five days following the burying of the mines, 12 passes were performed on the packed gravel and the sand roads (6 passes for each type of road). For each road, three passes were done during daytime and three during night-time. With the intent to evaluate the efficiency of the technology in optimum and poor conditions, the daytime passes were performed just after the morning transition period, at optimum day period, and just before the evening transition period [9]. Similarly, the three night-time passes were performed just after the evening transition period, at the optimum night period, and just

[8] A section of that road including the buried mine sites 1 to 5 (see Table VIII) was made of packed gravel.

[9] The exact timing of these passes relative to the exact moment of the heat flow inversion may slightly differ because of the geographic latitude difference between DRES and Wainwright and the natural day-to-day variations of the moments of these transitions.

before the morning transition period.

FIGURE 23 – Representative photographs of the packed gravel road used for the Wainwright trial

Each pass was performed with the trial vehicle and the THV-1000 LWIR camera. For each pass, two operators who had no more than two hours of practice in visual inspection of typical LWIR videos of buried mines and the author of this document were monitoring successively 20 minutes of video output from the IR camera, while the vehicle was travelling on one of the two types of road at a speed ranging between 2.5 and 3 km/h. During their IR video monitoring shifts, the operators used three different identification calls when suspicious sites appeared in the FOV of the camera: AT, AP and unknown. The identification "unknown" was used when suspect areas with strong thermal surface

FIGURE 24 – Representative photographs of the sand road used for the Wainwright trial

TABLE VII

Mine spatial distribution on the packed gravel road in the Wainwright trial

Site	Distance (m)	Position			Mine type
		left	centre	right	
1	180	1AT			1-TSUR
2	247		1AT		1-TSUR
3	386			1AT	1-TSUR
4	437			1AT	1-TSUR
5	567		1AT		1-TSUR
6	759			1AT	1-TMA3
7	902	1AT	1AT		1-TMA3/1-TM62
8	1030			1AT	1-M21
9	1124	1AT	1AT		2-TSUR
10	1195		1AT/1AP		1-MK7/1-VS50
11	1254		1AT	1AT	1-VS2.2/1-M21
12	1436		1AT	1AP	1-M21/1-VS50
13	1535		1AT		1-MK7
14	1712	1AT			1-MK7
15	1817			1AT/2AP	1-TMA3/2-PSUR
16	1999			1AT	1-MK7
17	2181			1AT	1-MK7
18	2235		2AP		2-PSUR
19	2286	1AT		1AT	1-MK7/1-TM62
20	2447	1AT		1AP	1-M21/1-VS50
21	2613		1AT		1-TMA3
22	2771			1AP	1-PMA3
23	2869	1AT			1-MK7
24	3067		1AT	1AT	2-M21
25	3165		1AT		1-M21
26	3255		1AT	1AT	1-MK7/1-TSUR
27	3401			1AT	1-TMA3
28	3587	1AT/2AP			1-M21/2-VS50
29	3658	1AT			1-MK7
30	3763		2AP		1-PSUR/2-PMA3
31	3862		1AT	1AT	2-TSUR
32	3979			1AT	1-M21
33	4069		1AT/2AP		1-M21/2-VS50
34	4213	1AT			1-MK7
35	4306	1AP		1AP	2-VS50
36	4458		1AP		1-PMA3
37	4652		1AT		1-M21
38	4850	1AP			1-VS50
39	4936		2AP	1AT	2-PMA3/1-M21

Notes: The numbers in the site and distance columns identify the buried mine sites and its distance from the starting point of the pass in metres. The position columns identify the class of mine and its approximative location across the road. The mine type column describes the type of mine buried (TSUR,PSUR: AT,AP surrogate) and the numbers preceding the acronyms define the quantities of the specified mines.

TABLE VIII

Mine spatial distribution on the sand road in the Wainwright trial.

Site	Distance (m)	Position			Mine types
		left	centre	right	
1	80	1AT			1-TSUR
2	174		1AT		1-TSUR
3	270			1AT	1-TSUR
4	390	1AT			1-TSUR
5	520		1AT		1-TSUR
6	719		1AT/2AP		1-TSUR/2-PSUR
7	812			1AT	1-M21
8	899			1AT	1-MK7
9	983			1AT	1-M21
10	1187		1AT		1-TMA3
11	1286	1AT/2AP			1-M21/2-VS50
12	1464			1AT/2AP	1-TSUR/2-PMA3
13	1526	1AT		1AT	1-TSUR/1-TMA3
14	1592			1AT/2AP	1-M21/2-VS50
15	1691	1AT			1-TMA3
16	1784	1AT		2AP	1-TSUR/1-PSUR/1-PMA3
17	1875			1AT	1-MK7
18	1994	1AT		1AT	2-TSUR
19	2118		1AT		1-TMA3
20	2194	1AT			1-MK7
21	2501			1AT/2AP	1-M21/2-PMA3
22	2682		1AT		1-MK7
23	2969	1AT			1-TSUR
24	3085			1AT	1-M21
25	3356	1AP		1AT	1-VS50/1-TSUR
26	3573	1AT		1AP	1-M21/1-VS50
27	3754			1AT/2AP	1-TSUR/2-VS50
28	3893	1AT			1-MK7
29	4047	1AT		1AT	2-TM62
30	4152	1AT		2AP	1-M21/2-PSUR
31	4266			1AT/2AP	1-MK7/2-VS50
32	4418	1AT			1-TSUR
33	4528	1AT		1AT	1-VS2.2/1-TSUR

Note: The columns are defined as in Table VII.

effects which might hide potential thermal volume effects were seen. An observer, positioned behind the operator, received a confirmation of the presence of buried mine sites in the FOV of the IR camera by communicating with the driver [10]; this allowed him to record successful detections pointed by the operator. Other functions of the observer were to tabulate all false detections called by the operator and also to report if himself was able to observe the IR signature of a buried mine when its presence in the FOV was confirmed by the driver. The information compiled by the observer was later analyzed in laboratory. During this analysis, identification calls (AT, AP, or unknown) reporting real buried mine sites were classified as successful detections. For burying mine sites showing large surface thermal effects covering multiple buried mines (AT or AP), all mines were considered detected when identified by the operator. Table IX reports quantitatively the detection efficiencies of the operators and the observer for the different types of mine and the false alarm rates compiled from the observer's notes. Furthermore, the types of thermal effects (surface, volume, or their combination) were evaluated from the IR video inspection made in laboratory and is reported as well in Table IX.

In addition to the video recording of the different passes, one IR digital image of the road was taken for each metre travelled over the first 3.5 km of road [11]. In parallel with the digital recording, the temperature profile of the ground was sampled each half hour. The probe was positioned at the beginning of the packed gravel road. Later in laboratory, the digital images were used to quantify the temperature contrasts of the different buried mines detected by the operator and the temperature gradients at a depth of 7 cm were derived with the method described in Section 2.4. Figures 25, 26, 27, 28, 29 and 30 show

[10] A system of stakes placed along the side of the road (outside the FOV of the IR camera) allowed the driver to identify precisely when a buried mine site was in the FOV of the camera.

[11] For some passes identified in Figs. 27 and 28, a computer breakdown prevented the digital recording of the IR images.

TABLE IX

Detection efficiencies and false alarm rates obtained in the Wainwright trial

Time	Per.	% of Detection											FA/10m			Det. Type (%)					
		AT							AP							AT			AP		
		All	S	M21	MK7	TMA3	TM62	VS2.2	All	S	VS50	PMA3	AT	AP	U	V	S	V+S	V	S	V+S
08:30-10:20	Oper.	55(40)	70(10)	25(12)	70(10)	60(5)	100(2)	0(1)	21(19)	40(5)	20(10)	0(4)	0.55	1.06	0.21	0	55	40	11	53	11
	Obs.	65(40)	90(10)	42(12)	70(10)	60(5)	100(2)	0(1)	32(19)	40(5)	20(10)	50(4)									
14:10-15:55	Oper.	80(40)	100(10)	83(12)	70(10)	60(5)	50(2)	100(1)	65(20)	60(5)	70(10)	60(5)	0.77	1.28	0.15	0	40	50	10	50	20
	Obs.	60(40)	60(10)	42(12)	60(10)	100(5)	50(2)	100(1)	75(20)	100(5)	70(10)	60(5)									
17:10-18:55	Oper.	68(40)	70(10)	58(12)	80(10)	60(5)	100(2)	0(1)	65(20)	60(5)	70(10)	60(5)	0.43	0.84	0.07	0	50	28	30	35	10
	Obs.	55(40)	70(10)	42(12)	50(10)	60(5)	100(2)	0(1)	45(20)	60(5)	50(10)	20(5)									

Day passes, gravel packed road (July 24,1995)

Time	Per.	% of Detection											FA/10m			Det. Type (%)					
		AT							AP							AT			AP		
		All	S	M21	MK7	TMA3	TM62	VS2.2	All	S	VS50	PMA3	AT	AP	U	V	S	V+S	V	S	V+S
08:15-09:50	Oper.	46(35)	67(15)	0(7)	17(6)	75(4)	100(2)	0(1)	0(16)	0(5)	0(10)	0(1)	0.78	0.89	0.07	37	0	11	0	0	0
	Obs.	49(35)	73(15)	0(7)	17(6)	75(4)	100(2)	0(1)	0(16)	0(5)	0(10)	0(1)									
14:40-16:20	Oper.	49(37)	81(16)	25(8)	33(6)	25(4)	0(2)	0(1)	15(20)	60(5)	0(10)	0(5)	0.45	0.83	0.11	41	8	11	30	0	0
	Obs.	60(37)	81(16)	38(8)	50(6)	50(4)	0(2)	100(1)	25(20)	60(5)	20(10)	0(5)									
18:20-19:55	Oper.	76(37)	100(16)	38(8)	50(6)	75(4)	100(2)	100(1)	45(20)	100(5)	10(10)	60(5)	0.37	0.90	0.18	73	5	3	45	0	0
	Obs.	76(37)	100(16)	38(8)	50(6)	75(4)	100(2)	100(1)	45(20)	100(5)	10(10)	60(5)									

Day passes, sand road (July 25, 1995)

Time	Per.	% of Detection											FA/10m			Det. Type (%)					
		AT							AP							AT			AP		
		All	S	M21	MK7	TMA3	TM62	VS2.2	All	S	VS50	PMA3	AT	AP	U	V	S	V+S	V	S	V+S
21:20-23:05	Oper.	68(40)	40(10)	75(12)	90(10)	60(5)	100(2)	0(1)	25(20)	60(5)	10(10)	20(5)	0.59	0.65	0.32	65	13	5	35	5	10
	Obs.	63(40)	40(10)	58(12)	90(10)	60(5)	100(2)	0(1)	50(20)	80(5)	30(10)	60(5)									
03:00-04:40	Oper.	100(40)	100(10)	100(12)	100(10)	100(5)	100(2)	100(1)	65(20)	100(5)	50(10)	60(5)	0.13	0.50	0.12	95	2.5	2.5	75	0	0
	Obs.	100(40)	100(10)	100(12)	100(10)	100(5)	100(2)	100(1)	75(20)	100(5)	70(10)	60(5)									
06:15-08:00	Oper.	93(40)	100(10)	75(12)	100(10)	100(5)	100(2)	100(1)	25(20)	40(5)	10(10)	40(5)	0.24	0.55	0.28	73	5	18	20	20	0
	Obs.	95(40)	100(10)	83(12)	100(10)	100(5)	100(2)	100(1)	40(20)	60(5)	30(10)	40(5)									

Night passes, gravel packed road (July 26-27,1995)

Time	Per.	% of Detection											FA/10m			Det. Type (%)					
		AT							AP							AT			AP		
		All	S	M21	MK7	TMA3	TM62	VS2.2	All	S	VS50	PMA3	AT	AP	U	V	S	V+S	V	S	V+S
21:15-22:50	Oper.	38(37)	44(16)	25(8)	17(6)	25(4)	100(2)	100(1)	20(20)	20(5)	10(10)	40(5)	0.24	0.60	0.84	38	14	0	20	0	0
	Obs.	51(37)	50(16)	38(8)	33(6)	75(4)	100(2)	100(1)	20(20)	20(5)	10(10)	40(5)									
03:00-04:40	Oper.	83(36)	100(16)	57(7)	66(6)	75(4)	100(2)	100(1)	40(18)	80(5)	13(8)	60(5)	0.24	0.47	0.22	78	5	3	35	0	5
	Obs.	83(36)	100(16)	71(7)	66(6)	50(4)	100(2)	100(1)	45(18)	80(5)	25(8)	60(5)									
06:10-07:45	Oper.	61(36)	80(15)	25(8)	50(6)	100(4)	0(2)	100(1)	25(20)	60(5)	10(10)	20(5)	0.20	0.37	0.22	49	0	14	20	0	5
	Obs.	61(36)	80(15)	25(8)	50(6)	100(4)	0(2)	100(1)	25(20)	60(5)	10(10)	20(5)									

Night passes, sand road (July 27-28, 1995)

Notes: The detection efficiencies are given for the operators and the observer for each mine type and overall (the numbers between parentheses are the quantities of buried mines included in the statistical evaluations). The false alarm rates are classified as AT, AP, or unknown as specified by the operators. The detection types (volume or (and) surface thermal effects) are evaluated independently in laboratory from the recorded videotapes.

the detection efficiency of the operator, the thermal effects (surface or volume) by which the buried mines were detected, the temperature contrasts of the detected buried mines and the temperature gradients which are derived from these acquired experimental data. For this compilation, the temperature contrasts may be the averages of multiple buried mines from a same site. The following sections address different aspects of the use of the IR technology to detect buried mines. These aspects were observed during this trial and are of interest for the ILDC program.

IR Detection over Shadowy Road

An important scenario investigated for the ILDC program in the Wainwright trial was the efficiency of IR technology to detect buried mine sites when close vegetation creates shadow on sections of the road. Unfortunately, a malfunction of the digital acquisition system during the daytime passes on the sand road prevented the gathering of quantitative data of this phenomenon. Nevertheless, these specific passes have been recorded on videotapes. From these video recordings and as reported by the operators, it has been observed that the presence of shadow covering partially the surface of the road complicates seriously the interpretation of the IR images. These difficulties are created by the large apparent temperature variations between the sunny and shadowy areas of the road which could be many times greater than the apparent temperature contrast associated with a buried mine site. The situation may be even more severe if the vegetation screens only partially the road and generates an intermingling of sunny and shadowy surfaces of size comparable with the searched IR signatures. However, as shown in Fig. 31, the formation of the IR signature of a buried mine is possible in shadowy roads sections.

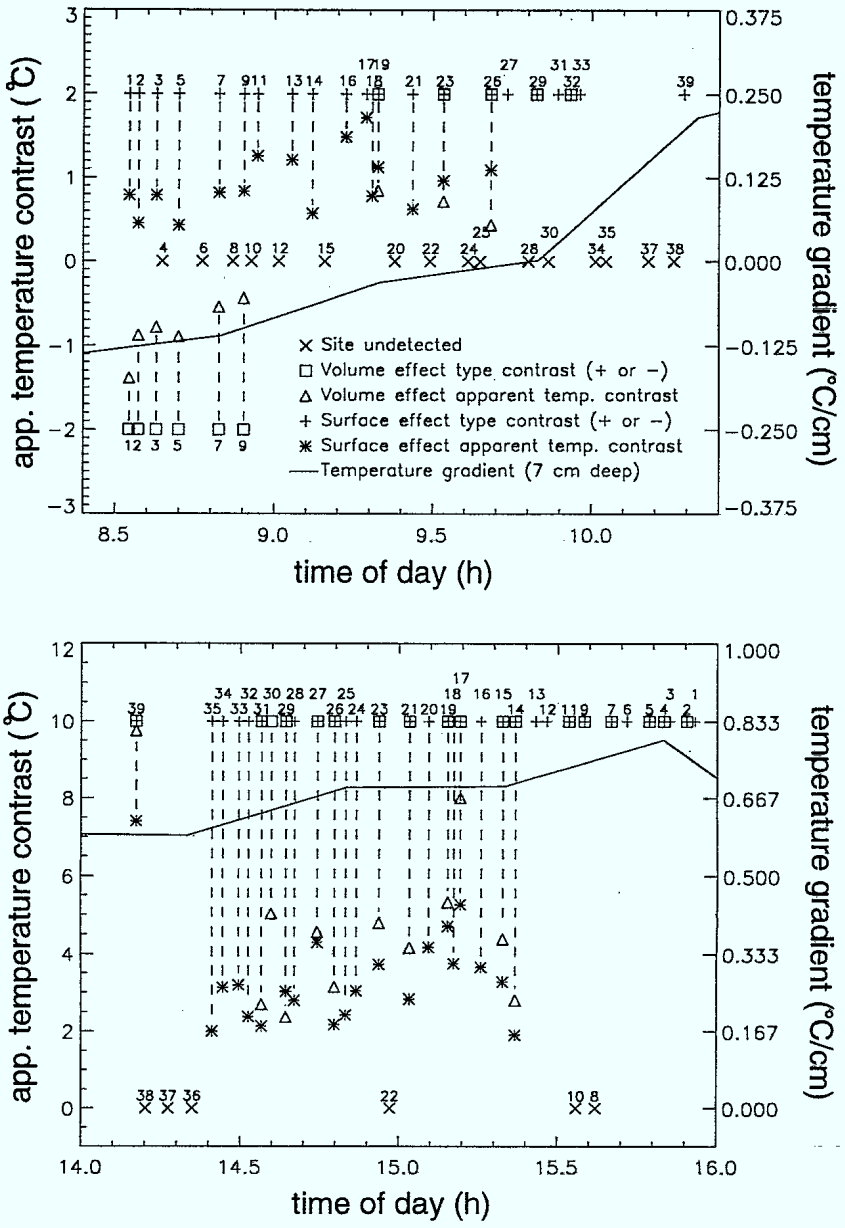

FIGURE 25 – Dynamic representations of the passes simulating the ILDC scenario in the Wainwright trial after the morning transition period (upper plot) and at the optimum daytime (lower plot) over the packed gravel road. The numbers identify the mine sites described in Table VII. The symbol definition list given in the upper plot describes also the lower plot. A quantitative evaluation of the detection efficiencies and of the false alarm rates for these passes can be found in Table IX.

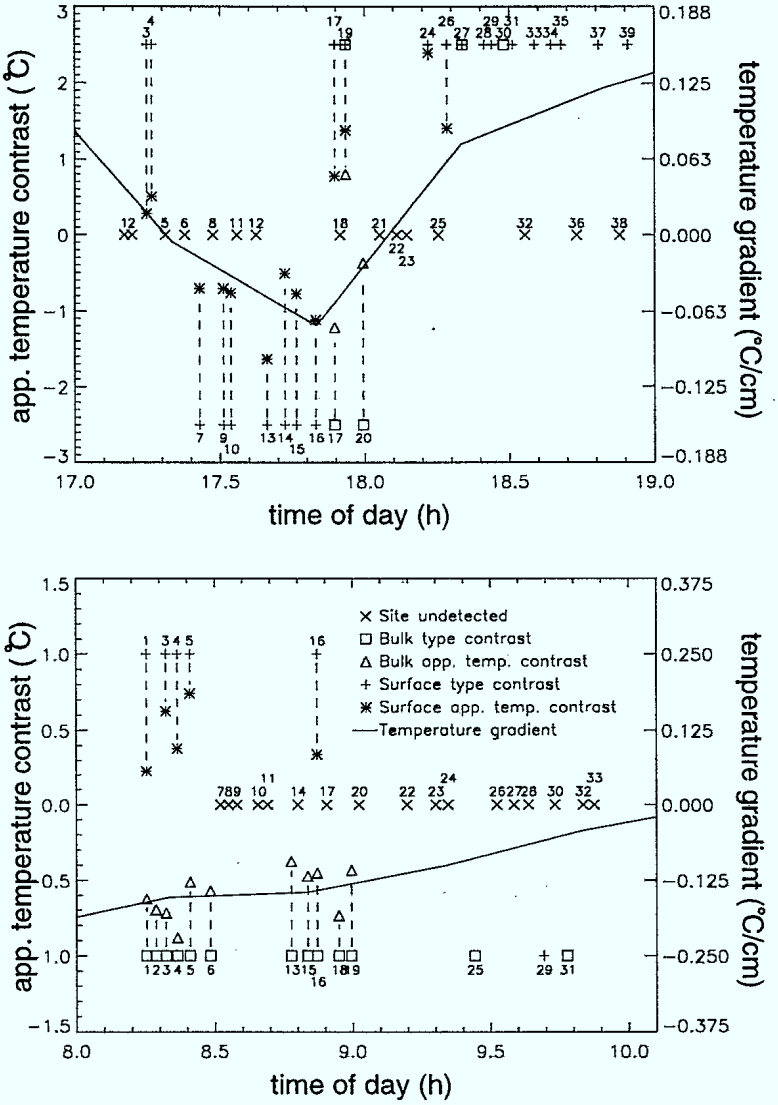

FIGURE 26 – Dynamic representations of the passes simulating the ILDC scenario in the Wainwright trial before the evening transition period over the packed gravel road (upper plot) and after the morning transition period over the sand road (lower plot). The numbers identify the mine sites described in Table VII for the upper plot and in Table VIII for the lower plot. The symbol definition list given in the lower plot describes also the upper plot. The sudden inversion observed in the temperature gradient curve between 17:15 and 18:15 (upper plot) coincides with a light rainfall. A quantitative evaluation of the detection efficiencies and of the false alarm rates for these passes can be found in Table IX.

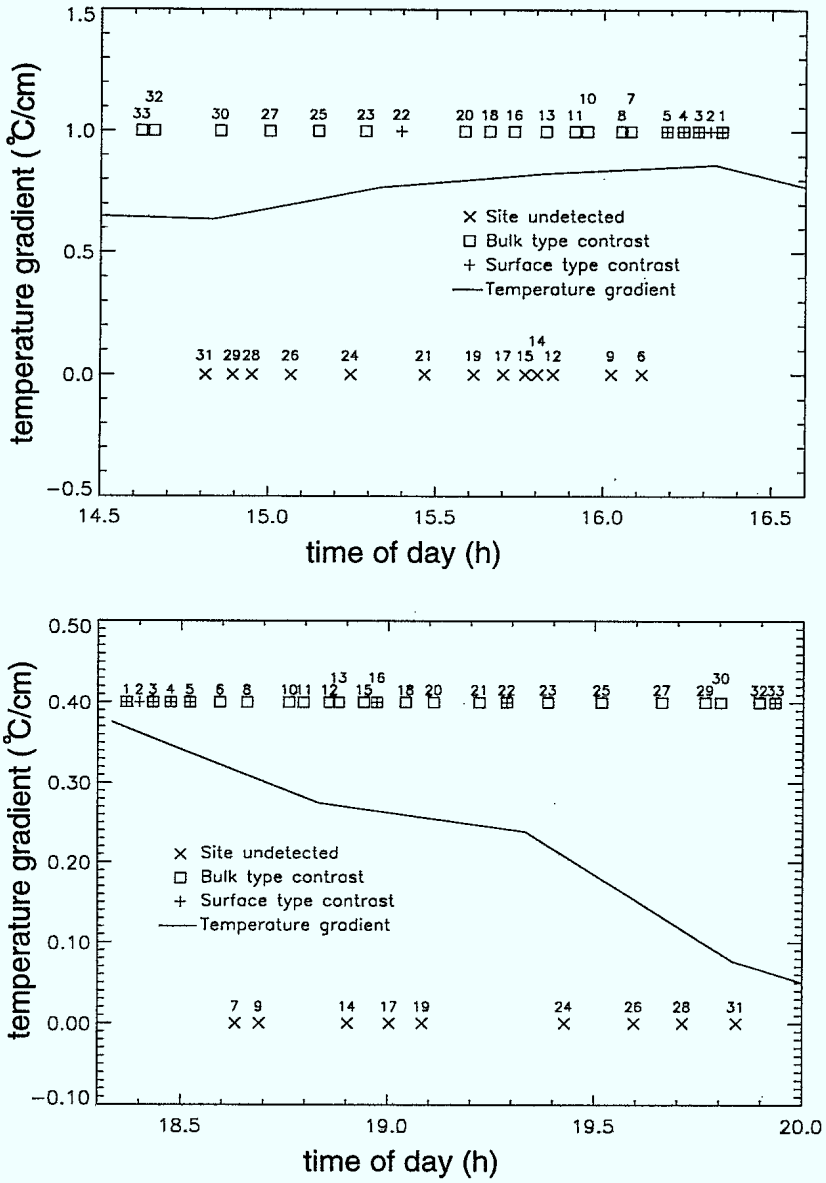

FIGURE 27 – Dynamic representations of the passes simulating the ILDC scenario in the Wainwright trial at the optimum daytime period (upper plot) and before the evening transition period (lower plot) over the sand road. The numbers identify the mine sites described in Table VIII. During these two passes, a malfunction of the digital acquisition system prevented the measures of the temperature contrasts of the buried mines. A quantitative evaluation of the detection efficiencies and of the false alarm rates for these passes can be found in Table IX.

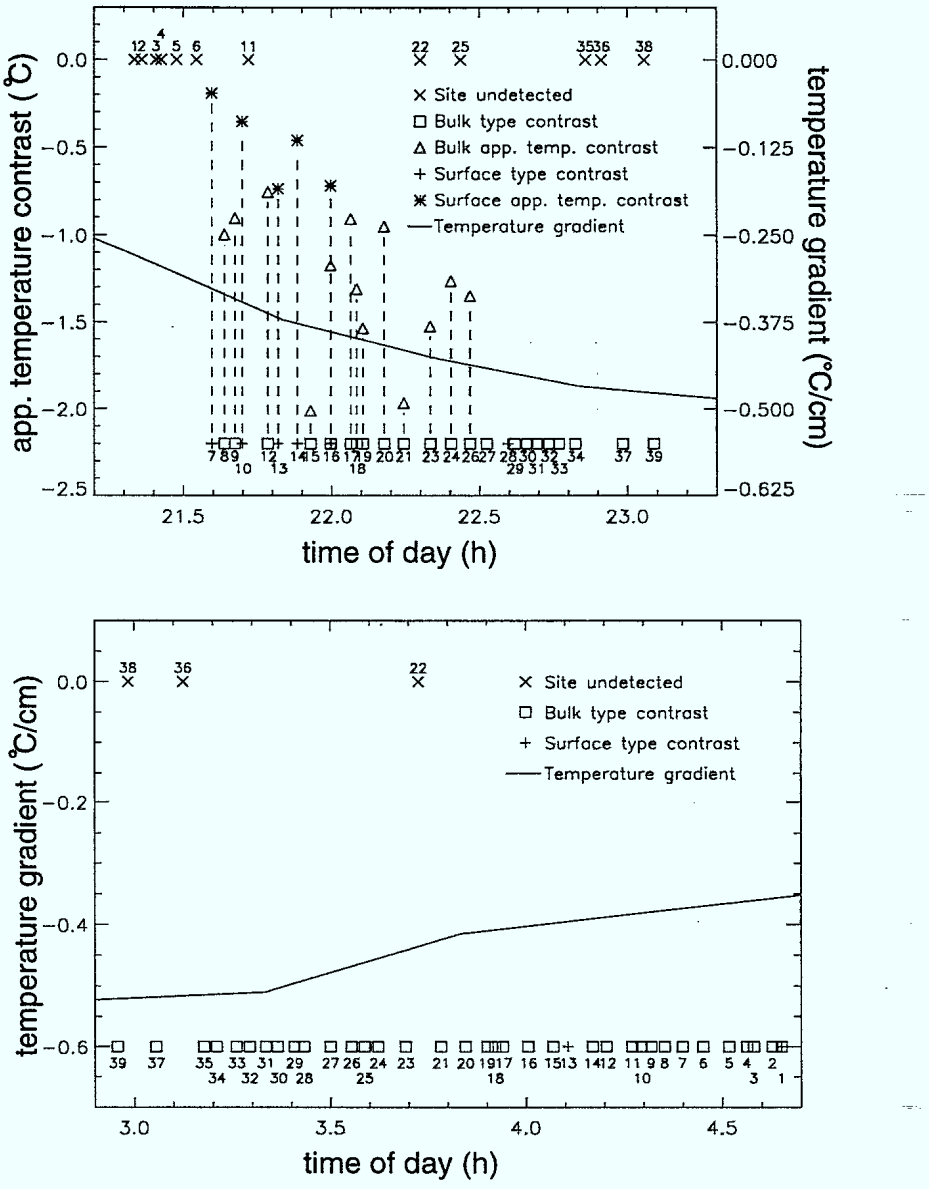

FIGURE 28 – Dynamic representations of the passes simulating the ILDC scenario in the Wainwright trial after the evening transition period (upper plot) and at the optimum night-time period (lower plot) over the packed gravel road. The numbers identify the mine sites described in Table VII. During the optimum night-time period, a malfunction of the digital acquisition system prevented the measures of the temperature contrasts of the buried mines. A quantitative evaluation of the detection efficiencies and of the false alarm rates for these passes can be found in Table IX.

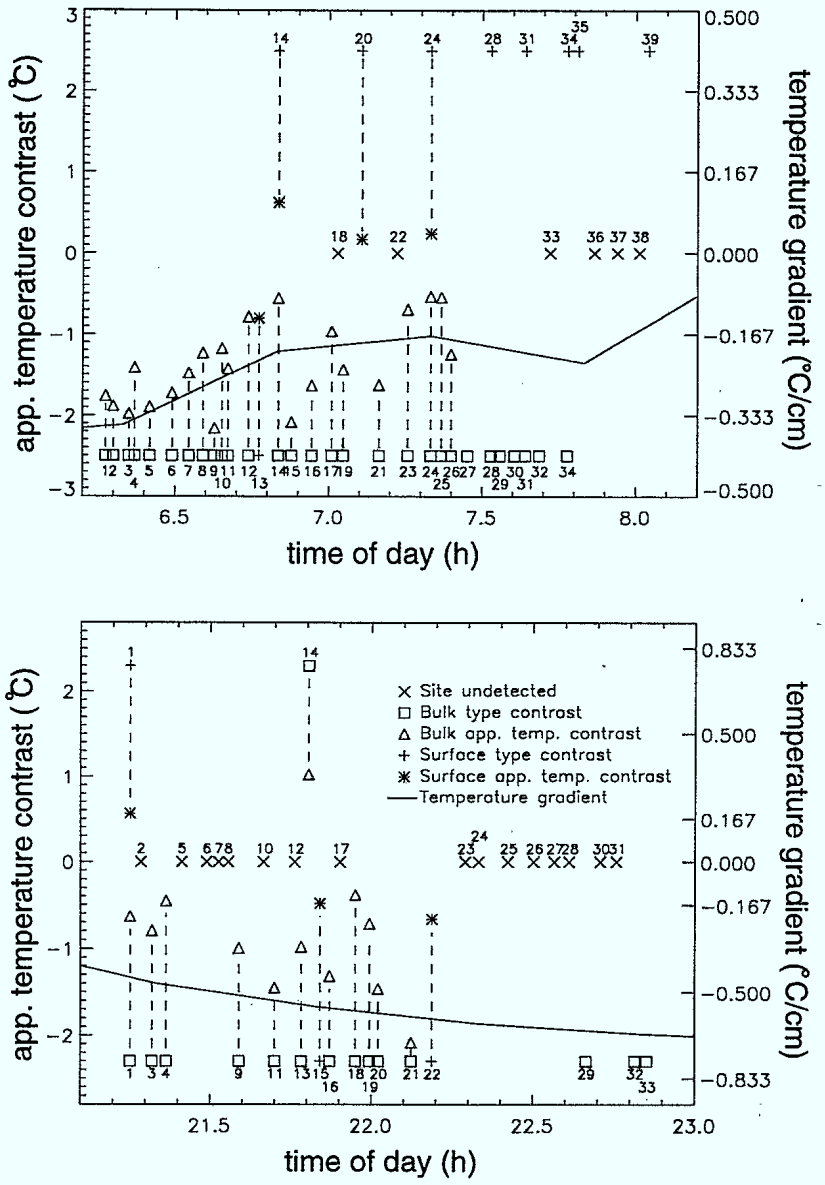

FIGURE 29 – Dynamic representations of the passes simulating the ILDC scenario in the Wainwright trial before the morning transition period over the packed gravel road (upper plot) and after the evening transition period over the sand road (lower plot). The numbers identify the mine sites described in Table VII (upper plot) and in Table VIII (lower plot). The symbol definition list given in the lower plot describes also the upper plot. A quantitative evaluation of the detection efficiencies and of the false alarm rates for these passes can be found in Table IX.

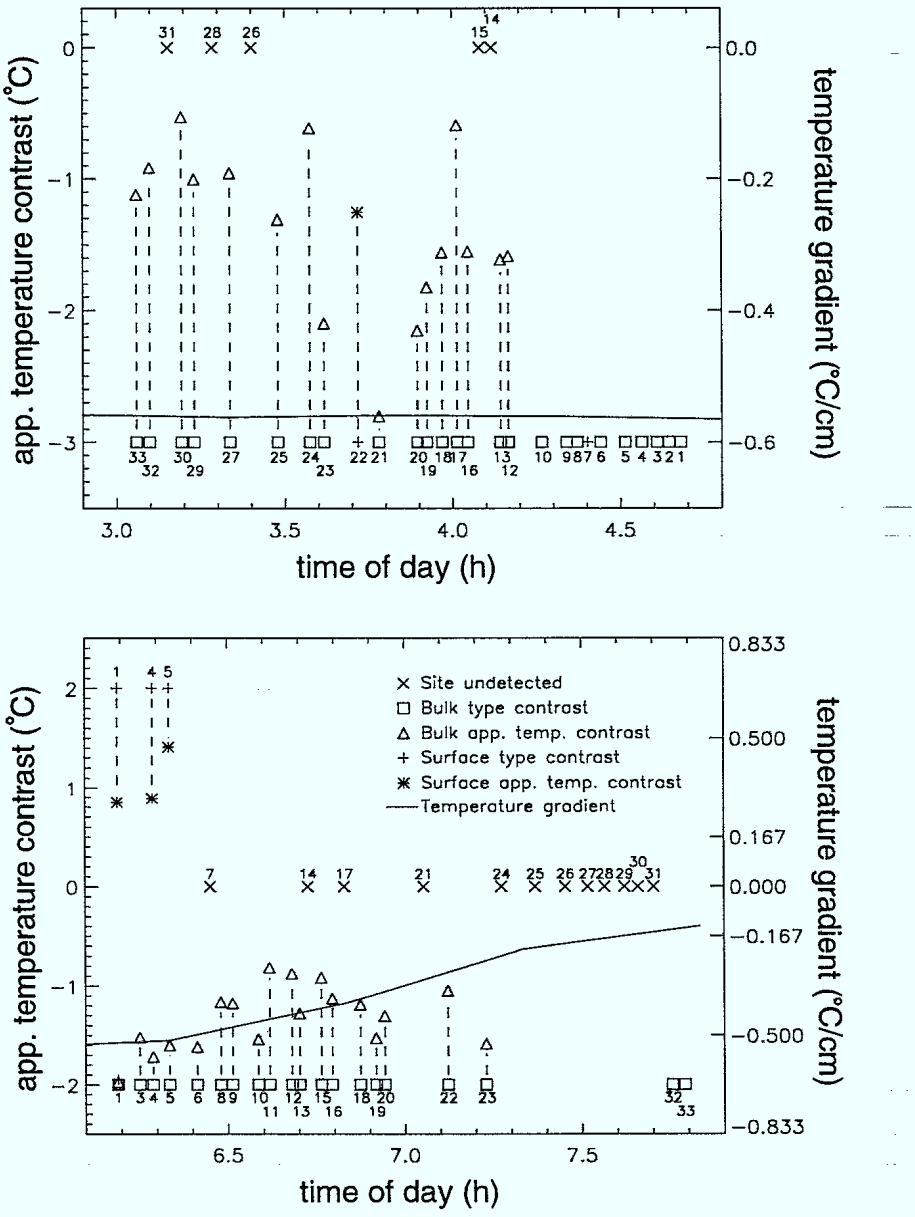

FIGURE 30 – Dynamic representations of the passes simulating the ILDC scenario in the Wainwright trial during the optimum night-time period (upper plot) and before the morning transition period (lower plot) over the sand road. The numbers identify the mine sites described in Table VIII. The symbol definition list given in the lower plot describes also the upper plot. A quantitative evaluation of the detection efficiencies and of the false alarm rates for these passes can be found in Table IX.

IR signature of an AT surrogate seen in a shadowy area

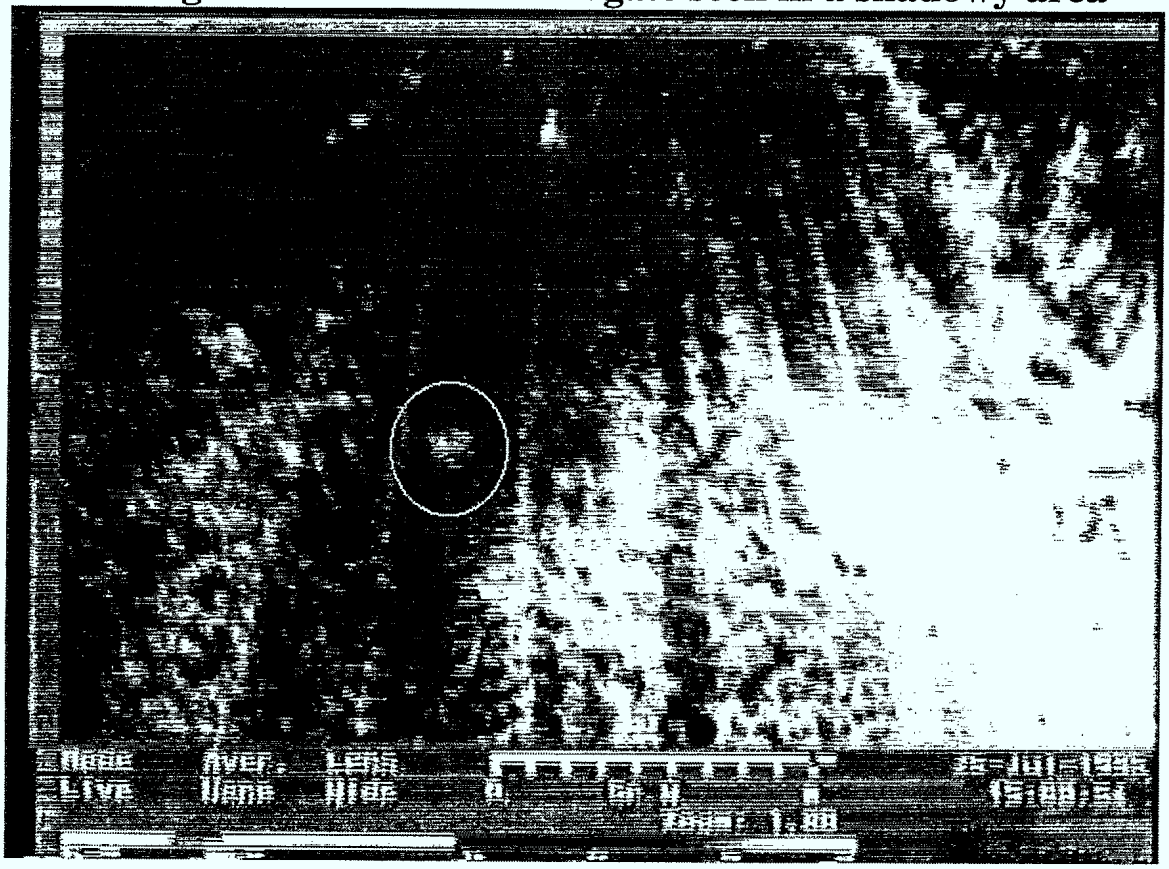

Wainwright, July 25 1995
Route #2, Sand Road
time: 15:09

FIGURE 31 – Picture of the IR signature of a buried mine on a shadowy section of a road (circled blob). This picture is digitized from the video output during the optimum daytime period over the sand road.

Spatial Correlation of the Temperature Gradient Measurements

For the trials preceding the Wainwright experiment, the temperature gradient mo nitoring parameter was always measured on one specific site. For a dynamic trial as the one reported in this section, it is easy to question the value of this measurement if the demining operation using IR technology is performed at great distance from the temperature probe. In order to evaluate this aspect of the monitoring technique, two temperatures probes were used in the Wainwright trial. The first probe, located at the beginning of the packed gravel road, acquired automatically the temperature profile of the ground each half hour. The second probe, also located on the packed gravel road but 3.5 km further than the first one, was sampled manually at different times during the 5-day trial. Figure 32 shows the temperature gradients obtained with the temperature profiles of these two probes. This plot shows, for the 15 manually temperature profiles sampled, a relatively good correlation. For more than 70 % of the cases, the temperature gradient differences between the two probes are less than 15 % or less than .1°C/cm. For the cases left, two of them show temperature gradient differences between 30 % and 35 % (star symbols identified with a triangle) and two others have a difference between 50 % and 60 %. These four important differences occurred at night.

Effect of the Wind on the Efficiency of Detection

One may observe, in Table IX, the poorer detection efficiency obtained during the optimum daytime (14:40-16:20) over the sand road when compared with the one performed close to the evening transition period (18:20-19:55). This can be explained by the high wind existing during that optimum daytime period. The wind over a sand road moves constantly the top layer of soil. As a consequence, the heat dynamic responsible for the

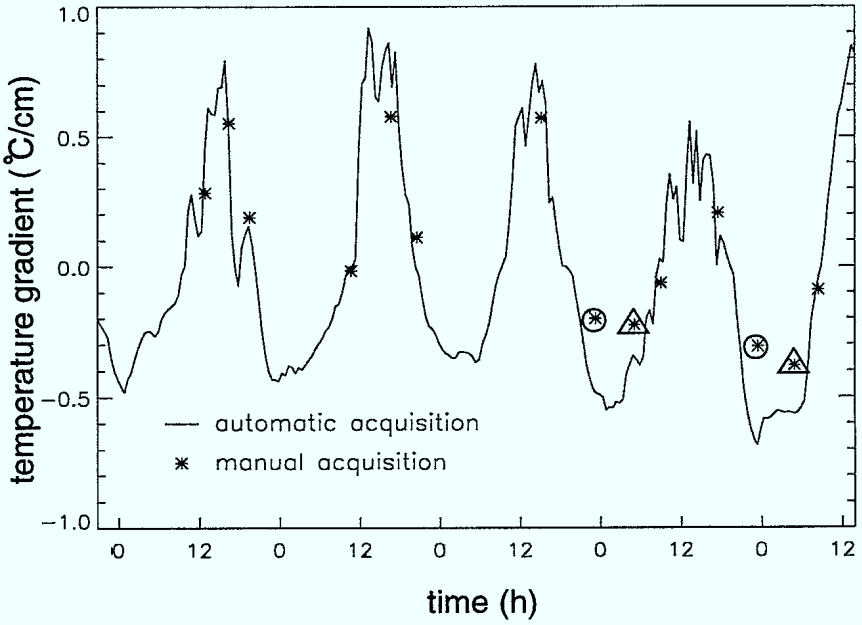

FIGURE 32 – Plot of the spatial correlation of the temperature gradients in the Wainwright trial. The continuous line reports the temperature gradients measured with the automatic acquisition system and the star symbols show the temperature gradients measured manually. The two measures were taken 3.5 km apart on the packed gravel road. The star symbols identified with triangles and circles point occurrences where the temperature gradients measured in the two sites differ by more than 30 % and 50 %, respectively.

formation of the buried mine IR signature do not have the time to stabilize and only weak temperature contrasts appear. This effect is even more important that the temperature gradient monitoring technique do not predict adequately this poor condition of detection (this last assertion is deduced by comparing the temperature gradient of these two passes in Fig. 27). Therefore, it is important to identify this environmental condition (wind over sand road) as one where the IR technology may perform poorly at detecting buried mines.

Effect of Road Grading on the IR Signature of Buried Mines

A secondary trial investigating the effects of grading packed gravel roads with heavy equipment on the buried mine IR signatures has been performed at the end of the Wainwright trial. The goal of this operation was to evaluate the level of deterioration in the formation of the buried mine IR signatures after serious perturbations in the overall thermal properties of the road. The reason for this test is the potential future needs identified by the ILDC program for road preparation before demining (this road preparation may become a necessity to protect the ILDC vehicle against booby traps). To obtain this type of information, a plough was requested from the Base. Then, we asked the driver to grad the road as he usually does for maintenance. In 45 minutes, he made three passes: two of these passes were intended to bring soils from the sides of the road to the centre and the last pass was done to even the moved soil. Thirty minutes after the last pass , the trial vehicle was used as before to evaluate the detection efficiency of IR technology. This pass with the trial vehicle was done near the optimum daytime period. The main results from this evaluation are:

- The IR signatures of buried mines are still easily observable after road grading as long as the total thickness of the soil above the buried mine is less than 10 cm as for the case of buried mines without hole effects (see Section 2.1).
- The effect of grading the road eliminates the thermal surface effect by making the soil surface uniform.
- The grading operation perturbs the thermal state of the road and a minimum period of half an hour is necessary before an acceptable thermodynamic equilibrium allowing the clear formation of the buried mine IR signatures is reached.

4.2.3 Spatial Structures Associated with the IR Signatures of Buried Mines

An interesting observation resulting from the Wainwright trial is the discovery of the spatial signatures associated with the IR blobs of specific buried mines. Figure 33 shows the example of the MK7 anti-tank mine. This mine shows regularly, for the different passes, a ring-shaped IR signature (white or black depending on the direction of the heat flow). It is assumed that this structure is closely related to the spatial variation of the heat conductivity across the thickness of the mine. Other geometric shapes, shown with less clearness, were also observed with other types of mines. These findings open the door to the possibility of identifying buried mines from the spatial aspect of their IR blobs.

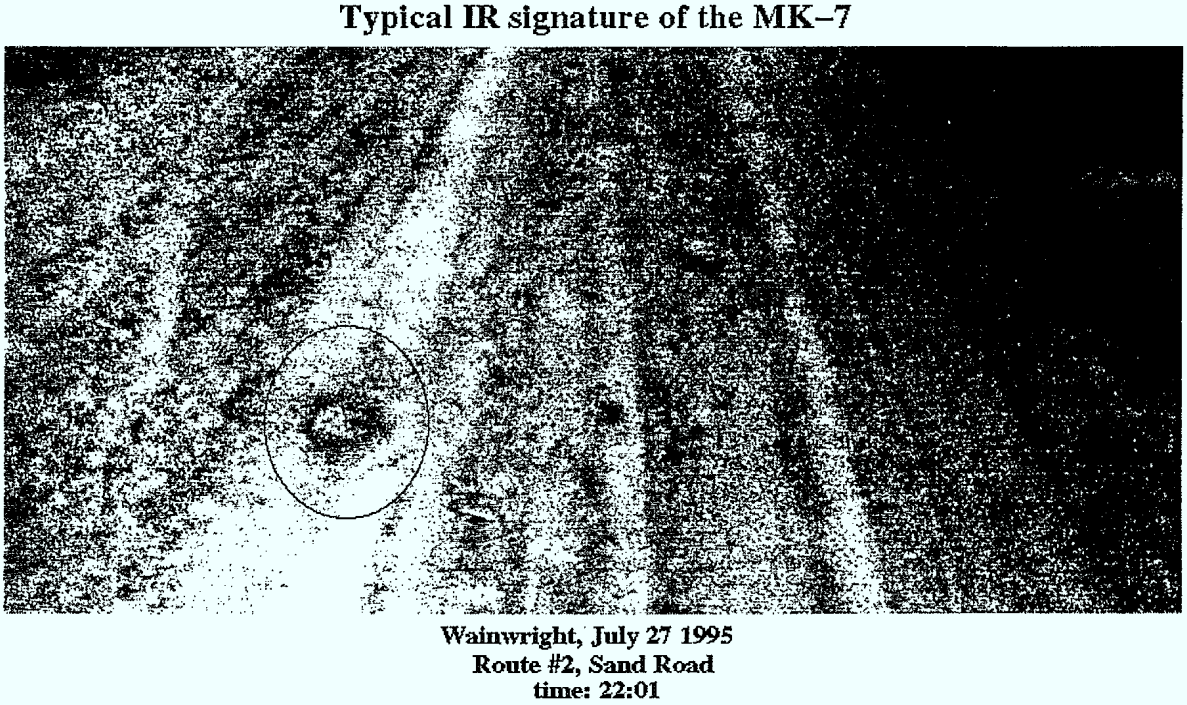

FIGURE 33 – Picture of the typical ring IR signature associated with the MK7 AT mine (circled blob)

Validity of the IR Signature Associated with the Developed Mine Surrogates

In Section 3.4, the description of the making of IR surrogates based on the use of the "Uniroyal Adiprene-100" to simulate the Yugoslavian TMA-3 anti-tank mine was introduced. This choice was based on the similar thermal characteristics between this material and TNT. In support of that design, Fig. 34 shows side by side the IR signatures of this AT surrogate and the TMA-3. Quantitative measurements from the digital image report a difference in contrast smaller than 30 %. This result tends to confirm, at least in a semi-dry environment, the validity of the use of this surrogate to simulate the IR characteristics of the TMA-3 when buried. The advantages associated with the use of these IR surrogates instead of the real TMA-3 are to simplify greatly the security precautions associated with the manipulation of real mines.

4.3 Miscellaneous Behaviours of Buried Mine IR Signatures to External Effects

This section reports the earliest experimental evaluations of IR technology used as a tool to detect buried mines for the ILDC program. For this trial, we use the THV-782 LWIR camera and a frame grabber to sample manually the images provided by the camera or in an automatic mode at specific time intervals. The site used is the same than the one described in Section 4.1 (Canadian Prairies site). However, the results shown in this section were gathered only a few days after burying the two TMN-46 surrogates. The behaviours of the buried mine IR signatures in response to the external effects (natural or artificial) investigated in this trial were analyzed to answer important questions posed by the ILDC project team. Most of these interrogations originate from the possible need for a road preparation procedure before demining. Some of the questions to which answers have been found with this trial are shown below. For each answer, a series of IR images describing

IR Signature of the TMA–3 and the IR Surrogate

Wainwright, July 28 1995
Route #2, Sand Road
time: 04:08

FIGURE 34 – Picture of the IR signatures associated with the AT surrogate and the TMA3 (circled blobs). This evidence tends to confirm the validity of the designed AT surrogate.

the time evolution of the effect investigated is referred. All the experimental results were obtained during the optimum daytime period on a packed gravel road.

What is the effect of vehicle traffic on the IR signatures of the buried mines ?

This question may appear inappropriate because mines are designed to detonate when a vehicle is passing over them. This would be the case for a standard vehicle. However, the vehicle developed for the ILDC program is especially designed to show a tire ground pressure below the detonation threshold of usual AT mines. With this capability introduced, it is important to evaluate the effect of the passage of vehicles on the IR signatures of the

buried mines. To evaluate this aspect, the effect associated with the passage of a "Bison" (a Canadian personnel carrier vehicle) over a packed gravel road was investigated [12]. As shown in Fig. 35, the modification of the IR signatures of the buried mines generated by this vehicle is minimal.

What is the effect of chain sweeping on the IR signatures of the buried mines ?

This interest originates from the possible need to clear the road from booby traps. For that investigation, a chain was held across the road by a "U" type rack and was pushed by a low ground pressure vehicle over the buried mine site. Figure 36 shows four IR pictures of the buried mine site before and after "chain sweeping" the road. It is observed, for a low IR contrast situation, that the effect of chain sweeping affects only slightly the IR signatures of the buried mines.

What is the effect of road sweeping on the IR signatures of the buried mines ?

With the possible road preparation procedure, an interest for improving the IR detection of buried mine sites by sweeping the loose gravel off the road was introduced. This question undermines also that loose gravel spreading may be a method of reducing the detection efficiency of the IR technology and sweeping the road may reduce the effect of this countermeasure. Figure 37 shows four IR pictures of a buried mine site before and after sweeping. The site was first generously covered with loose gravel. On that picture, one can see the serious camouflage effect resulting from this action. On the second picture, we observe that the IR signatures disappear immediately after the action of sweeping the road. Then, less than 40 minutes later, the IR signatures of the buried mines are back and show much better spatial definitions. With this result, it is obvious that sweeping the loose

[12]Using a "Bison" instead of the ILDC vehicle establishes an upper limit (a Bison is much heavier than the ILDC vehicle) for the effect of the passage of a low ground pressure vehicle on the buried mine IR signatures.

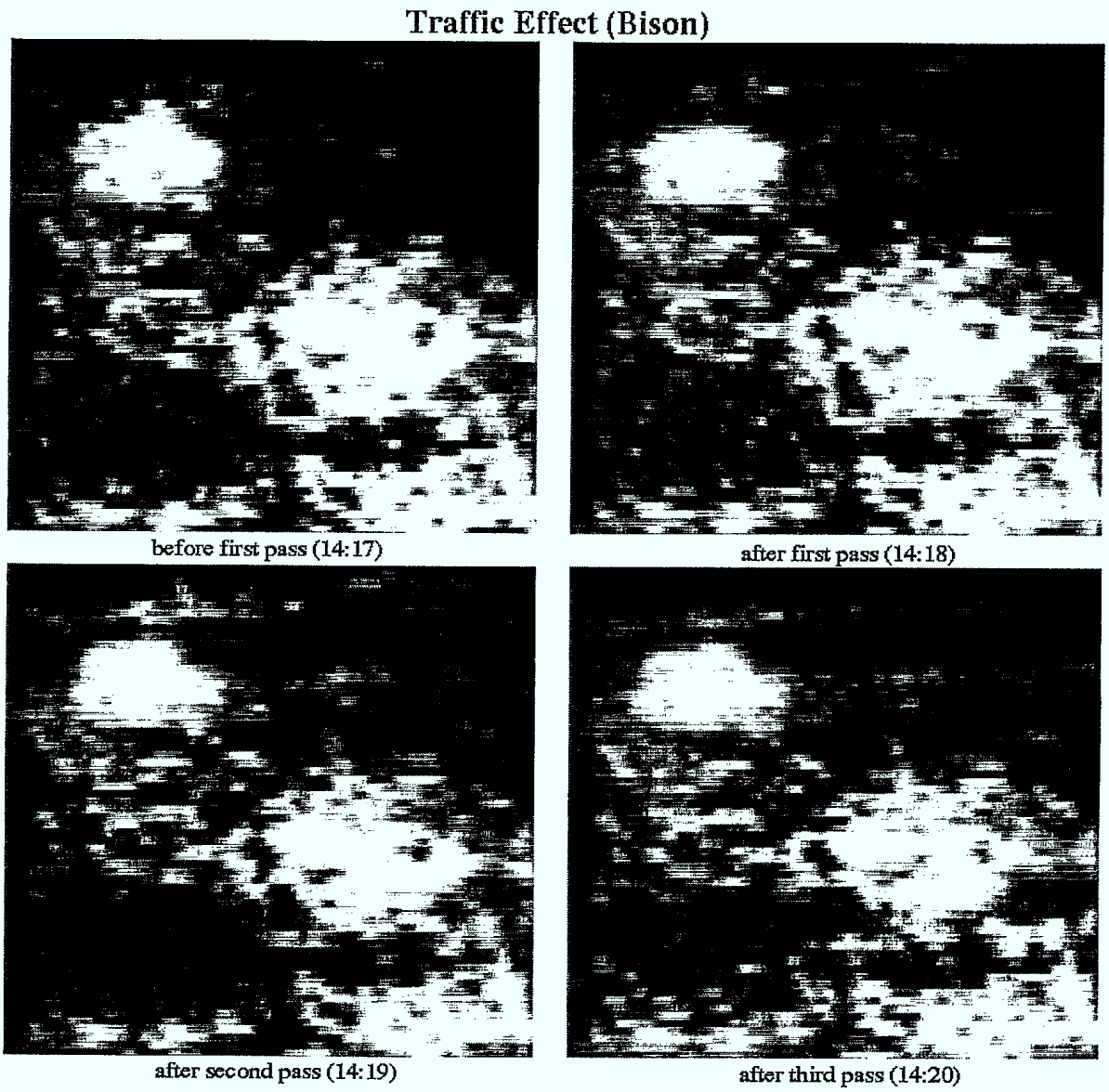

FIGURE 35 – Effect of vehicle traffic on the IR signatures of buried mines. Pictures of the effects of the passage of a "Bison" (a Canadian personnel carrier vehicle) on the IR signatures of the buried mines on a packed gravel road. As observed, the effect of low intensity vehicle traffic is minimal on this type of road.

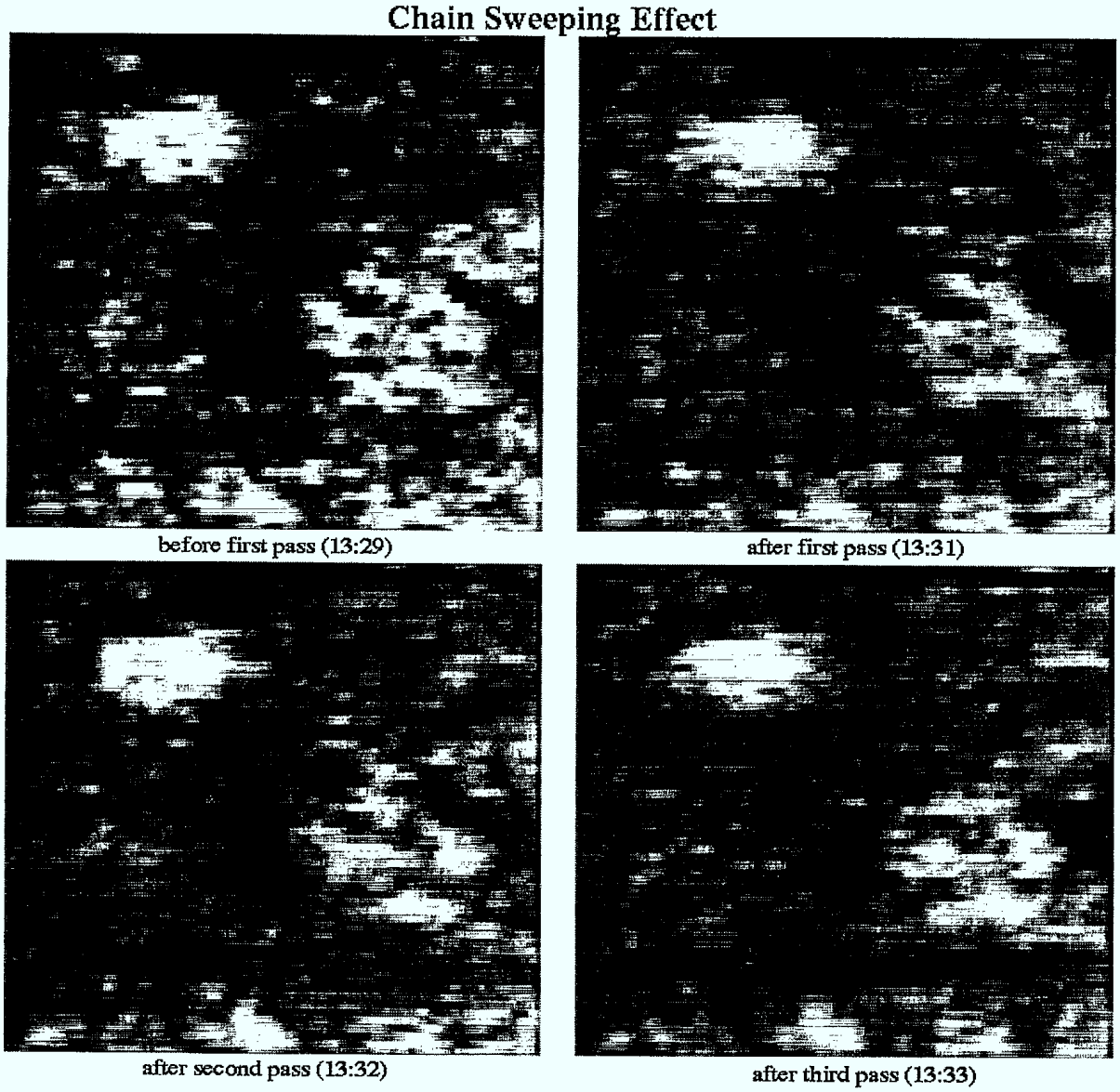

FIGURE 36 – Effect of "chain sweeping" on the IR signatures of buried mines. Pictures of the effect of the passage of a low ground pressure vehicle pushing a "U" type rack holding a chain across the packed gravel road. For this low IR contrast situation, it is observed that this action affects only slightly the contrast of the IR signatures of buried mines.

gravel off a packed gravel road produces beneficial effects on the IR detection efficiency.

Observation of a Temperature Contrast Anomaly

In Chapter 2.0, the daily evolution of the temperature contrasts of buried mines are described as four distinct periods: optimum daytime, evening transition, optimum nighttime and morning transition periods. However, this representation of the temperature contrast daily evolution describes only a general behaviour. Figure 38 shows the occurrence of a temperature contrast anomaly. This anomaly was created by the approach of dark grey clouds associated with a cold front. The effect of this anomaly is to seriously modify the heat exchange state between the soil and the atmosphere, which completely erases the temperature contrasts of the buried mines for almost an hour. After that period, the heat exchange between the atmosphere and the soil came back to a new heat exchange state allowing the return of the IR contrasts of the buried mines. This kind of phenomenon supports the need for a monitoring technique as the measure of the temperature gradient in the soil to predict unexpected situations as this one where IR detection technology may perform poorly.

4.4 MWIR Trials

At the early stage of the ILDC program, it was necessary to purchase rapidly an IR camera to evaluate the capability of this technology to detect buried mines. At that moment, it was decided, based on published literature and accumulated expertise, to acquire a LWIR camera. However, as the experimental evaluation of the LWIR camera (the THV-1000) evolved, it became important to compare its detection capacity with an MWIR camera. To achieve this comparison in an acceptable fashion, the THV-1000 LWIR camera and the IR-M500 (and subsequently the IR-M600) were positioned side by side on

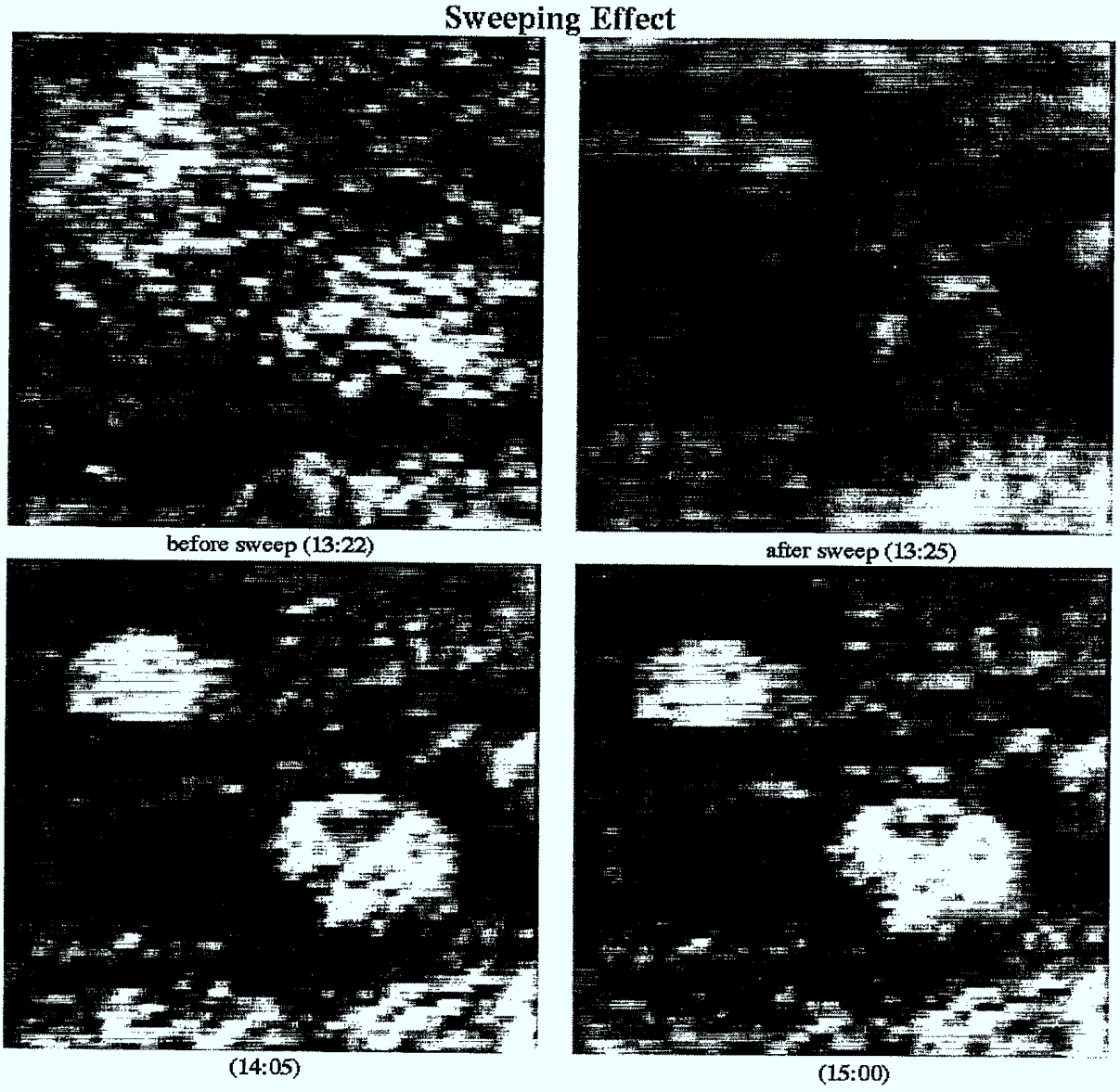

FIGURE 37 – Pictures of the effects of sweeping the loose gravel off the road. Beside a short period after sweeping where the IR contrasts disappear, one can observe that sweeping the loose gravel off a packed gravel road improves the temperature contrasts and the spatial aspects of the IR signatures of the buried mines.

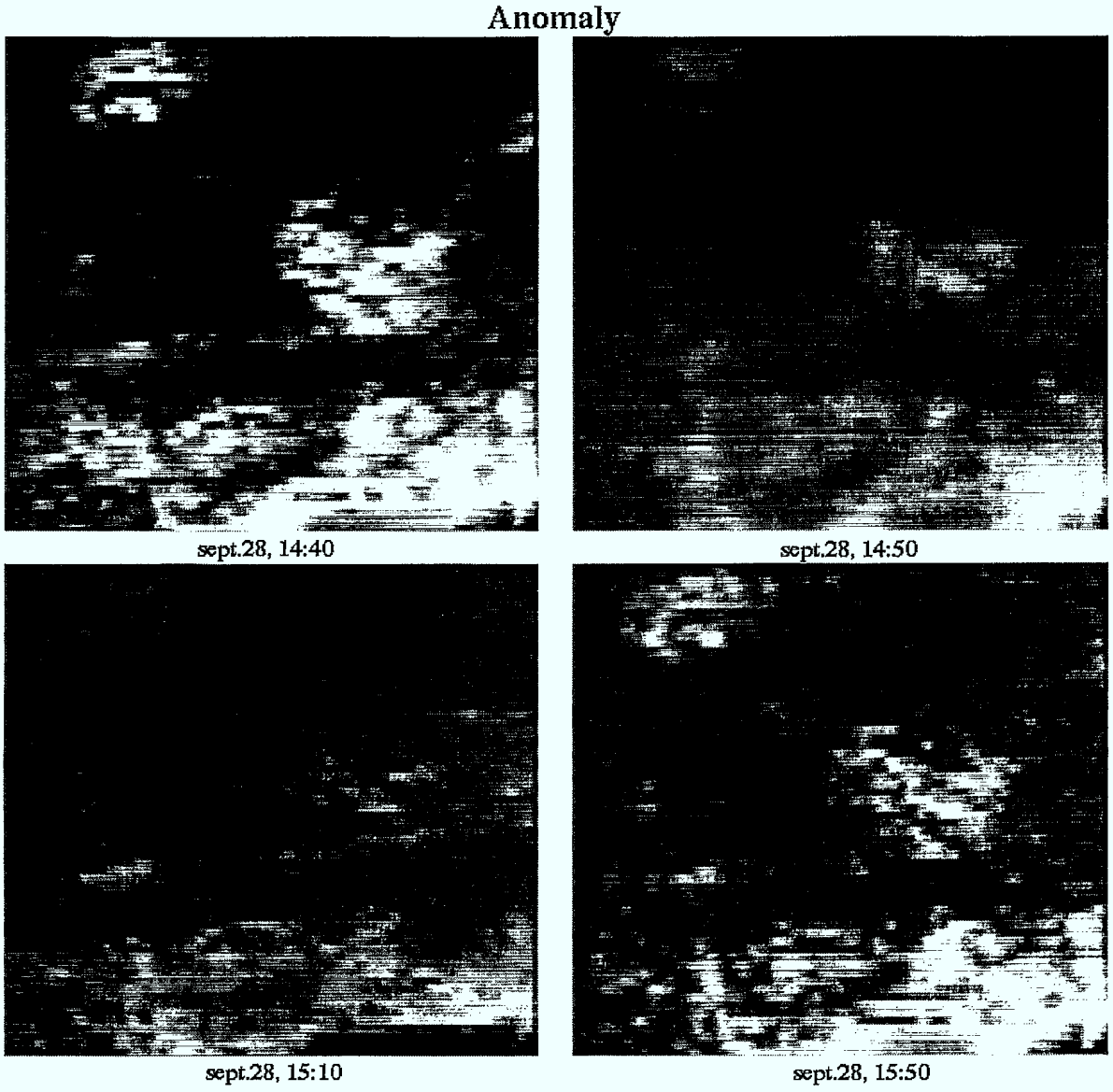

FIGURE 38 – Pictures of the effects of drastic weather changes on the IR contrasts of the buried mines. The effect of this anomaly (the approach of a cold front) is to stop the heat exchange between the atmosphere and the ground, which contributes to reduce strongly (almost completely) the IR contrasts of the buried mines. After the passage of the cold front (more than one hour later), heat exchanges between the atmosphere and the soil are re-established and the IR contrasts of the buried mines reappear.

the camera holder of the trial vehicle described in Section 3.3. Then, multiple passes on the "Radar Road" trial site were performed during optimum day and optimum night periods. This trial took place in October 1995. The results of this comparison trial are summarized in Table X and in the following comments.

TABLE X

Comparison between the THV-1000 and the IR-M600

	IR-M600	THV-1000
Temperature sensitivity (1)	limited	good
Input capability (2)	limited	good
Output capability (3)	limited	good
Image quality (4)	best	good
Robustness (5)	good	good
Cost (6)	~US$90k	~US$105k

Notes: The numbers between parentheses refer to the comments below.

(1) From visual inspection of the night-time video recordings, the two cameras present sensibly the same intrinsic temperature sensitivity even at environmental temperatures as low as -10°C. However, it has been observed by inspecting the daytime video recordings that the MWIR camera shows much higher sensitivity to extrinsic temperature noise. It is believed that this higher extrinsic noise sensitivity originates from the higher sun radiation content in the MWIR band, which increases the apparent temperature clutters of the soil surface. It may be possible to reduce this effect by using optical filters. However, the use of filters will also reduce the incoming radiative signal which may deteriorate the intrinsic temperature sensitivity.

(2) The IR-M600 presents less flexibility for the grey mapping adjustments of the output image than the THV-1000. Also, the IR-M600 do not have standard communication compatibilities for remote control application. This reduces seriously its

capability to be integrated in a centralized control station.

(3) The IR-M600 camera does not give access to the full-scale internal digitized signals contrary to the THV-1000. That limits severely most image postprocessing and thermographic quantitative measurements made outside the original dedicated processing boxes.

(4) The nominal image resolution taken at the RS-170 outputs of the two cameras should be quite similar based on the technical specifications stated by the two companies. However, the Focal Plane Array (FPA) technology used by the IR-M600 provides a better stabilized (clearer) images than the THV-1000.

(5) **ILDC Notes**: Following the manufacturer's specifications, it appears that the Mean Time Between Failure (MTBF) of the LWIR camera is dictated by the lifetime of the Stirling cooler as it is the case for the MWIR camera. That implies, if the cameras react similarly to the working environment, that the two IR imagers should show comparable MTBF (see Tables II and III).

(6) **ILDC Notes**: The prices shown, dated June 1996, are for the basic package (camera head, remote control, power supply) and include wide field of view lenses.

5.0 DISCUSSION

In the previous chapters, many theoretical and experimental results are reported. For most parties interested in the described subjects, it may appear difficult to withdraw the main principles emerging from these accumulated information. To reduce these difficulties, the present section aims at summarizing the principal consequences associated with the use of LWIR imaging technology to detect buried landmines. The discussed concepts are referred to the specific supporting experimental results or theoretical models and are presented especially to answer already identified questions of interest for the Improved Landmine Detection Capability (ILDC) committee.

A) What are the basic phenomena at the origin of the IR signature of buried landmines ?

The IR signature of a buried landmine is essentially associated with a temperature difference at the soil surface between the buried mine site and its immediate surroundings, as described in detail in Section 2.1. This temperature difference results from two mechanisms: the local increase of the soil heat impedance and the heat exchange cycle between the atmosphere and the soil. The first mechanism, the soil heat impedance change associated with buried landmines, can be related to surface and (or) volume thermal effects. The surface thermal effect is related to the formation of a disturbed thin layer of soil on the surface of the buried mine site which shows a poor thermal contact with the deeper soil layers. This thin layer of soil is created by the human activities associated with the action of burying the mine. The surface thermal effect is highly sensitive to atmospheric radiation level, provides a poor spatial information about the exact position of the buried mine (signature can easily cover 1 m^2 area), last only few days (depending on weather conditions),

and does not occur on uncompacted roads (as sand roads). On the other hand, the volume thermal effects are related to the high heat impedance of the mine (a few times higher than the one associated with the soil) and the higher heat impedance associated with the disturbed soil covering the mine itself (which is named the hole effect). These volume thermal effects provide usually precise information on the position of the mine and even on the mine itself (see Subsection 4.2.3). This is also the predominant effect responsible for the buried mine IR signature at night. The hole effect can last for a few months depending on weather conditions and is not present on uncompacted roads as sand roads. As noted in a previous report (Ref. 8), if the IR signature of a buried mine is related to the presence of the mine exclusively (no surface or hole effects), the temperature contrast associated with the mine becomes undetectable when the mine is buried at depths greater than 10 cm. The second mechanism at the origin of the formation of the buried mine IR signature, the heat flow between the atmosphere and the soil, follows a 24-hour cycle which can be split into four distinct sequences: the optimum night-time period during which the heat flow is maximized from the soil to the atmosphere, the optimum daytime period during which the heat flow is maximized from the atmosphere to the soil, and two transition periods during which the heat flow changes direction (morning and evening transition periods). These four periods represent well on average the heat exchange evolution cycle but can be altered by specific weather conditions.

B) How the IR signature of a buried mine is detected ?

The difference in temperature associated with a buried mine site is detected by a thermal imager (or IR camera). A thermal imager measures the apparent temperature, which is the product of the emissivity and the absolute temperature. A method of characterizing the efficiency at which the thermal imager detects the apparent temperature difference

of a buried mine is the ratio between the apparent temperature contrast associated with the buried mine and the background noise observed in the IR image. Better is this ratio, better will be the detection efficiency (and lower the false alarm rate) of a human operator monitoring the IR images or an automatic target detection (ATD) algorithm. The first parameter defining the detection efficiency, the temperature contrast associated with a buried mine, is essentially dictated by the mechanisms described in the previous paragraph: the heat impedance difference and the heat flow between the atmosphere and the soil. On the other hand, the background noise of an IR image may originate from intrinsic or extrinsic noise sources. The intrinsic noise sources are associated with the IR camera itself and are characterized by the technical specifications of the camera (as the NETD). The extrinsic noise sources are mainly related to the fast spatial variation of the apparent temperature in the IR scene. This spatial variation of the apparent temperature is directly related to the atmospheric radiation level (mainly sun radiation). That is why we usually name this type of noise "radiation cluttering" and is the dominant noise source during daytime. The fact that the IR image background noise is dictated by the intrinsic noise during night-time and by the extrinsic noise during daytime, which is usually greater than the intrinsic noise for efficient thermal camera, explains the higher apparent temperature contrast threshold of detection during daytime reported in Table VI. This background noise phenomenon supports the higher detection efficiency and lower false alarm rate reported during the night-time periods in the Wainwright trial (Subsection 4.2.2).

C) What are the efficiency and false alarm rate expected from IR buried land-mine detection technology ?

Because of the environmental effects on the magnitude of the heat flow between the atmosphere and the soil (see the paragraph answering question A)), the detection efficiency

and the false alarm rate vary greatly with the time of day at which the technology is used. From the Wainwright trial (Subsection 4.2.2), which has been designed to simulate the operational scenario addressed by the ILDC project, the detection efficiency fluctuates (see Table IX) from around **40 %** to close to **100 %** for anti-tank mines and from less than **10 %** to more than **60 %** for antipersonnel mines buried on packed gravel and sand roads. During that trial, we have observed an important improvement of the detection efficiency during night-time because of the lower radiation cluttering noise at that period and over packed gravel road. We believe that the higher detection efficiency on the packed gravel road compared with the sand road is related to the exclusive presence of the thermal surface effect and the hole effect over the first type of road. Also from that trial, the false alarm rate (all types together) varies from **0.02** $\mathbf{m^{-2}}$ to **0.06** $\mathbf{m^{-2}}$. Once again, the lowest false alarm rate are observed during night-time where the radiation cluttering noise is minimized.

D) What are the environmental impacts on IR detection technology ?

As pointed out in the answers to Questions A and C, the main factor dictating the efficiency of the technology is the magnitude of the heat flow between the atmosphere and the soil. Beside the time of day, this heat flow can be affected in many ways. One of them is by a rainfall. The main effect of rain is to modify the thermodynamic equilibrium state of the soil by adding matter at a different temperature. If the rainfall is important, the modification to the heat flow dynamic can be sufficient to completely erase the IR signatures of buried mines. However, it has been observed (Ref. 16) that a light rainfall may improve the detection efficiency. It is believed that this improvement is related to the radiation cluttering noise reduction by soil surface water flushing. These conditions, even if the heat flow between the atmosphere and the soil is reduced, may still result with an improvement of the apparent temperature contrast to background noise ratio.

Another mechanism altering the heat flow between the atmosphere and the soil is the presence of insulating layers at the surface of the soil. Examples of natural insulating layers are fresh snow or dead vegetation. However, it has been observed that compact snow is not a severe limitation to the formation of the IR signature of a buried mine if that snow is not too thick (see the results of January 18, 1995, p. A5). Adding artificially loose gravel on a buried mine site will also act as an insulating layer and will show some camouflage properties (see Sweeping Effect, p. 75). However, the spreaded loose gravel will also show surface thermal effect if the time period since the spreading is not too long (a few days).

Another environmental effect reducing severely the IR signature of mines buried on sand roads is the wind (see the description entitled "The effect of the wind on the efficiency of detection" on page 69). The action of the wind is to regularly move the thin sand layer at the surface of the soil, which does not allow the formation of a stable IR signature. On packed gravel road, this wind effect on the IR contrasts of buried mines is negligible.

The effect of the presence of shadowy areas on the road has been investigated (see the description entitled "IR Detection over Shadowy Road" on page 61). As reported by an other work (Ref. 16), the IR signature of a buried mine, even if reduced, can be seen on shadowy surfaces. It is believed that the real difficulties associated with this situation is the necessary contrast adjustments to present in an optimum fashion the IR scene to the human operator and the possible increase of false alarms, depending on the shape of the shadow.

Finally, it is important to note that the atmospheric temperature (cold or warm) is not an absolute limiting factor in the formation of IR signature as observed in the results shown in Figs. 19, 20, 21 and 22. A parameter more related to the formation of this

signature is the atmospheric temperature difference between day and night. However, this method has the disadvantage of being imprecise and not sensitive to weather anomalies as the one shown in Fig. 38. Fortunately, as described in the paragraph of Question E, there is a simple technique allowing a direct and fast monitoring of the heat flow between the atmosphere and the soil.

E) Are there any ways of improving IR detection technology ?

There are two important actions which will improve significantly the performance of IR technology to detect buried landmines: perform demining operations during night-time and monitor the soil temperature gradient. It is understood that night-time demining may be difficult to achieve if not impossible, depending on the operational scenario. Nevertheless, it has been observed from direct measurements (see the paragraph entitled "Human IR Detection Threshold Measurements" on page 39) and from operational simulations (see quantitative results from the Wainwright trial in Table IX) that the contrast to background noise ratio of the night-time IR images allows an easier identification of the buried mine sites (thus improving detection efficiency) and that the false alarm rate is significantly reduced during that period (see Table IX).

On the other hand, the soil temperature gradient monitoring method described in Section 2.4 demonstrated a good correlation with the magnitude of the buried mine IR signature created by the volume thermal effects (see the results in Sections 4.1 and 4.2). This monitoring technique has the advantages of characterizing directly the heat flow between the atmosphere and the soil, while taking into account the soil heat impedance. However, a serious limitation of this technique is the spatial correlation validity of the measure. Because of the variation of the weather conditions over large distances, especially in regions

with rapid geographic changes (as mountainous areas), the measure of the soil heat flow may vary significantly with the increasing distance and affect the prediction efficiency of this technique. The level of this correlation has been evaluated in the Canadian Prairies (see the description entitled "Spatial Correlation of the Temperature Gradient Measurements" on page 69). It was observed, for a separating distance of 3.5 km, that 70 % of the temperature gradient measurements were equivalent within 15 %. It is interesting to observe that the greater relative differences were all observed at night [13]. At the present time, it is believed that characterization technique may not relate precisely the temperature gradient to the IR contrast of a mine buried at a specific depth, but should identify in an acceptable manner the optimum periods (optimum day and optimum night periods) during which the IR detection technique performs at its best. It is also believed that this characterization technique should be helpful in the detection of weather anomalies. In that direction, more work needs to be done to define satisfactory temperature gradient thresholds that would correspond to acceptable thermal contrast for the detection of buried mines. These thresholds may depend on the type of road investigated and the expected depths of the buried mines to detect.

F) What would be the effects of a "road preparation" procedure on IR detection technology ?

At the beginning of the ILDC project, the need for preparing the road before a demining operation was identified. The function associated with this road preparation procedure is to neutralize booby traps and antipersonnel mines which may be handled poorly by the ILDC detection vehicle. With that possibility, a question arises: will this procedure affect the performance of IR detection technology.

[13] It is difficult to relate with certainty this discrepancy to a night-time phenomenon or to a numerical evaluation artifact.

For simple road preparation procedure in which only chain sweeping or vehicle traffic are involved, we have verified experimentally (see Section 4.3) that their effects on the IR detection efficiency of buried mine sites are negligible. We have also verified that the effect of grading completely the road (as for packed gravel road maintenance) only eliminates the surface thermal effect without completely eliminating the IR signature of the buried mine if the soil cover thickness is not too large (see the description entitled "The Effect of Road Grading on the IR Signature of Buried Mines" on page 71). However, we can anticipate from the description of the basic phenomena at the origin of the formation of the IR signatures of buried mines that the use of a severe road disturbing tool as a military flail will seriously increase the number of surface and volume thermal distortions and may increase the false alarm rate to a level that makes the IR detection technique inapplicable. This effect should be important only on compacted roads where surface and volume effects are important.

Beside the negative aspects, there are potential advantageous operations for IR detection which may be performed by the road preparation vehicle. A first, one is sweeping any insulating layers off the road (see the sweeping effect in Section 4.3). A second one is to increase the radiation absorption of the road by using black paint. This action has the advantages of increasing the heat flow into the ground and of making uniform the road surface emissivity. Finally, another potential function performed by the preparation vehicle could be to produce a drizzle on the road to reduce the radiation cluttering noise. Even if these actions by a road preparation vehicle may improve the efficiency of the IR detection technique, they are not necessary to achieve an acceptable performance level.

6.0 CONCLUSIONS

With the increasing threats of low and nonmetallic buried landmines during peace-keeping operations, the capabilities of passive IR imaging technology as a mine detector has been extensively investigated under the Improved Landmine Detection Capability (ILDC) program. For the last year and a half, multiple trials have been performed at different periods of the year and the day on packed gravel and sand roads in different parts of Canada.

With the information acquired from these trials, basic models are established to improve the understanding of the formation of the buried mine IR signature. From this study, two basic variables, the heat flow between the atmosphere and the soil and the impedance anomaly created by the buried mine, have been identified as the main factors dictating the contrast of these IR signatures. Furthermore, two thermal effects behind the impedance anomaly created by the buried mine, the surface and volume thermal effects, have been observed and characterized in relation with the surrounding parameters (time, weather, and burying depth). It is observed that the surface effects and the hole effect, one of the components contributing to the volume effects, last a few weeks and a few months, respectively, after the burying operation. Furthermore, from previous work (Ref. 8) and also from some results shown in this report, it is verified that if only the presence of the mine contributes to the IR signature, this signature becomes undetectable if the mine is buried at a depth greater than 10 cm.

Also from these basic models, a technique, the temperature gradient measurement, is identified as a valid tool allowing the prediction of the performance of IR detection technology by monitoring the heat flow between the atmosphere and the soil.

In parallel with the improvement of the understanding of IR detection technology, many of the reported trials, which were designed to simulate as close as possible the operational scenarios addressed by the ILDC program, allow a precise practical evaluation of the capacity of IR imaging technology to detect buried mines. Fundamental parameters as the apparent temperature contrast thresholds of detection for a human operator (0.5-0.6 ^{0}C at night and 2-2.5 ^{0}C during the day), the detection efficiencies (40-100 % for AT and 0-75 % for AP), and the false alarm rates (.02-.06 m^{-2}) are reported in relation with time of day, type of road, and under winterlike conditions. From these trials, significative improvements of these fundamental parameters were observed at night, when the IR radiation cluttering is minimal, and over packed gravel roads. Also, a series of observations on the behaviour of IR detection technology under specific surrounding conditions of interest to the ILDC program are reported. The most important ones are: the effect of shadowy roads that may degrade the capacity of the operator to recognize a buried mine site if the shadow covers only partially the road in the FOV of the IR camera, and a strong wind that reduces detection efficiency over unpacked roads (as sand roads).

Finally, in view of the results reported in this document, it is believed that passive IR imaging would be a valuable detection technology when included in a multisensor vehicle as the one developed by the ILDC program and impressive performance can be achieved with this technology under the optimum conditions identified in this document.

7.0 ACKNOWLEDGEMENTS

The author would like to thank the people who made possible the different trials performed to test IR technology in the ILDC program: CWO Bill Maclean (DRES), Capt. Dave Rutky (DRES), 2lt Lieutenant Alexandre Paris (DRES), Messrs. Robert Ellingson (DRES), Wayne Syroviak (DRES), Jack Toews (DRES), Darell Boechler (DRES), Jean Dumas, Roger Fortin, WO Claude Lagace, and Mr. David Green (CDC). I would also like to recognize the computer support provided by Messrs. Kevin Russell (DRES), Lyle Sidor (DRES), and Dr. Vic Aitken (DRES). Finally, special thanks are addressed to Richter Enterprises and Mike Mays (Mitsubishi) for graciously providing us with MWIR cameras for comparison purposes.

8.0 REFERENCES

1. Nelsen, C., "Airborne Minefield Detection and Reconnaissance System (AMIDARS)", Proceedings of SPIE: Airborne Reconnaissance X, San Diego, CA, USA, August 1986, pp. 9-13.

2. Lareau, A. G., "Flight Performance of an Airborne Minefield Detection and Reconnaissance System", Photogramm Eng Remote Sens, Vol. 57, No.2, February 1991, pp. 173-178.

3. Johnson, S. R., "Minefield Reconnaissance and Detector (MIRADOR) Utility Study"", Wackenhut Advanced Technology Corp., Final Technical Report, Cont. DAAK70-88-D-0015, September 1989.

4. Miles, B. H., Cespedes, E. R., and Goodson, A. R., "Polarization-Based Active/Passive Scanning System for Minefield Detection", Proceedings of SPIE No. 1747: Polarization and Remote Sensing, San Diego, CA, USA, July 1992, pp. 239-252.

5. Muczynski, J. N., Horner, R. J., Mohan, P. L., and, Salinger J. A., "Remote Minefield Detection System (REMIDS) Real-Time Processing Architecture Study", Environmental Research Inst. of Michigan (ERIM), Technical Report, ERIM-208600-1-T, October 1988.

6. Del Grande, N. K. and al., "Dual-Band Infrared Capabilities for Imaging Buried Object Sites", Proceedings of SPIE No. 1942: Underground and Obscured-Object Imaging and Detection, April 1993, pp. 166-177.

7. Del Grande, N. K., "Sensor Fusion Methodology for Remote Detection of Buried Land Mines", Proceedings of the 3rd National Symposium on Sensor Fusion, Orlando, Florida, USA, April 1990.

8. Simard, J. R., "Experimental Evaluation of the Apparent Temperature Contrast Created by Buried Mines as Seen by an IR Imager (U)", DRES Report, No. 607, 1994 UNCLASSIFIED.

9. Waschl, J. A., "A Review of Landmine Detection", (U), DSTO Report, DSTO-TR-0113, 1994, RESTRICTED.

10. Jacob, P. A. M., "Simulation of the Thermal Behaviour of a Target and Its Nearby Surroundings", TNO Publication, PHL-1980-08, 1980.

11. Steinmanis, J. E., "Thermal Properties Database of Canadian Soils", Geotherm Inc., Technical Report, December 1989.

12. Patel, D. L., "Handbook of Land Mines and Military Explosives for Countermine Exploitation", United States Army, Technical Report (Defense Purposes Only), USA-BRDEC-TR // 2495, March 1992.

13. Firdaouss, M., "Determination of the Thermal Diffusivity of a Dry Soil from the Temperature *in situ* Measurement", C. R. Acad. Sc. Paris, Vol. 297, No. 2, September 1983, pp. 105-108.

14. Omega Inc., "Omega Complete Temperature Measurement Handbook and Encyclopedia", Corporative Handbook, First Edition, 1988, pp. T5-T18.

15. Data Translation Inc., "Data Translation DT707A/DT717 User Manual", Technical Report, 4^{th} Edition, February 1992.

16. Dumas, J., "Mesure de signatures infrarouges de mines terrestres et expériences de perception", DREV R-9525, juin 1996, SANS CLASSIFICATION

APPENDIX A

Winter Trial Specific Descriptions

In this appendix, specific remarks gathered during the winter trial are reported. Information as date, time, and weather conditions for a specific pass are given. Also, specific notes about the conditions under which the pass has been done may be provided. These short descriptions are grouped by month (December or January) and time of day (day or night) at which the passes were done.

Enumeration of the Specific Descriptions for Each Pass Identified in Fig. 19:

1. **Dec. 1, 1994, 16:00**: First pass after burying the mine surrogates. In the last few hours, large amount of snow melted living large moisture inhomogeneities across the road easily observable with the IR camera. A possible reason for the higher AP detection efficiency may be related to their shallow depths.

2. **Dec. 2, 1994, 15:00**: Small amount of snow fell through the day. Wind blowing and accumulation of snow on part of the road. First observation of buried mine IR signatures cover by compressed snow (under the tire prints of the trial vehicle).

3. **Dec. 3, 1994, 15:00**: Scattered cloud. Light snow (between 0.5 and 1 cm thick) covering the road more or less uniformly. First observation of the effect of snow cover on detection and false alarm rates.

4. **Dec. 5, 1994, 15:00**: Clear and sunny day. Snow cover has reduced but still distributed accumulations on sections of the road. Situation in which grazing sun rays

create important surface thermal cluttering. Volume thermal effect are negligible, but buried mine sites easily detectable by surface texture effects. However, as described in the text at the beginning of the section, this effect is deliberately ignored. Because of high cluttering, false alarms are not evaluated.

5. **Dec. 7, 1994, 15:35**: Situations very similar to the previous ones (Dec. 5, 1994, 15:00). Last pass of the month with snow traces on the road.

6. **Dec. 8, 1994, 14:10**: First pass where the surface thermal effect is considered as a valid detection tool. Even if identified as detected, most AP IR blobs cannot be distinguished from the AT IR blobs (see Fig. 14 for the position of the AP mines relative to their associated AT mines).

7. **Dec. 12, 1994, 15:00**: Clear and sunny with a light breeze. Situations similar to Dec. 8 (daytime).

8. **Dec. 15, 1994, 15:00**: Partially cloudy and warm breeze. Situations similar to Dec. 8 and 12. However, a few AP IR blobs begin to be distinguishable from their associated AT IR blobs.

9. **Dec. 19, 1994, 14:50**: Windy with thinly scattered cloud. Situations similar to Dec. 8, 12 and 15 (daytime). However, for this pass and the following ones, the criterion for AP mine detection has changed. It is now necessary to have a separated AP IR blob to be identified as detected. In this pass, no AP IR blobs are clearly distinguishable.

10. **Dec. 22, 1994, 15:00**: Warm and sunny day with light wind. Situations similar to Dec. 8, 12, 15 and 19 (daytime) but with good volume thermal effect. Only distinguishable AP IR blobs are considered as detected.

Enumeration of the Specific Descriptions for Each Pass Identified in Fig. 20:

1. **Dec. 2, 1994, 5:00**: First observation of the advantages associated with night-time observation: AT and AP IR blobs show clearly the positions and shapes of the buried mines, false alarm appears less severe than daytime. No snow.

2. **Dec. 5, 1994, 5:00**: Road state similar to the Dec. 2 pass (night-time) but with small snow accumulation on some sections of the road. First impressive volume thermal contrast observed during night-time.

3. **Dec. 6, 1994, 5:15**: Similar remarks to the pass of Dec. 5 (night-time).

4. **Dec. 7, 1994, 5:00**: A case of poor night thermal contrast. No obvious reason explaining this result. May be a case in which the temperature gradient measurement technique would be useful as a predicting tool. Still some snow patches left on sections of the road.

5. **Dec. 8, 1994, 5:00**: Clear sky with light wind. First night pass without snow traces on the road. Moderate thermal contrasts.

6. **Dec. 12, 1994, 5:00**: Frost on grass and trees, clear sky. Again, a case of poor night thermal contrast.

7. **Dec. 15, 1994, 5:00**: Light frost and clear sky. Frost seems to affect some IR blobs by altering locally their heat dynamic states. Beside the buried mine sites touched by the frost effect, one of the best thermal contrast observed so far.

8. **Dec. 19, 1994, 5:00**: Clear sky. Special situation in which most buried mines show a positive IR contrast. This effect has to be associated with the special heat dynamic state existing at that moment between the soil and the atmosphere. There are also few occurrences of AP IR blobs showing a negative thermal contrast.

9. **Dec. 22, 1994, 5:00**: Strong wind and mostly cloudy sky. Again, a situation of positive thermal contrast during night-time. However, the thermal contrast do not seem as high as Dec. 19 (night-time).

Enumeration of the Specific Descriptions for Each Pass Identified in Fig. 21:

1. **Jan. 03, 1995, 15:00**: Sunny day with a light breeze. Frost on the road with snow traces. A case in which the thermal contrasts (volume and surface) are poor.

2. **Jan. 10, 1995, 16:00**: Overcast sky. Pass where the overcast reduces greatly the sun radiation cluttering effect. IR images look almost like those obtained in night passes but with positive contrast. Also, occurrence once again of one buried mine site with a negative contrast.

3. **Jan. 11, 1995, 15:40**: Overcast day with medium fog. Once again, impressive situation in which the videotape looks like it has been done during night-time but with a positive IR contrast. The contrast is not as pronounced as the ones obtained

during the best passes, but the low level of cluttering associated with the weak direct sun radiation improves greatly detection efficiency and false alarm rate.

4. **Jan. 12, 1995, 15:35**: Overcast day with medium fog. Similar comments to the pass of Jan. 10 and 11 (daytime). Few occurrences of negative IR contrasts.

5. **Jan. 16, 1995, 15:45**: Overcast day where a layer of snow about 2.5 inches thick covers uniformly the road. See only the tire prints left by the trial vehicle in the morning pass. Only traces of IR blobs associated with buried mines are observable over the tire prints.

6. **Jan. 18, 1995, 14:25**: Sunny day. To investigate the phenomenon of the formation of the buried mine IR signature covered by compressed snow, the road has been back bladed in the morning leaving less than 2 cm of compressed snow (soil exposed in some areas). Thermal contrasts observed are weak, but the uniform layer of snow creates a flatness in the IR images, which reduces the false alarm rate.

Enumeration of the Specific Descriptions for Each Pass Identified in Fig. 22:

1. **Jan. 03, 1995, 5:05**: Frost and light snow on road, clear sky. Again, a case of good night thermal contrast. Most buried mines not detected are hidden by snow patches.

2. **Jan. 04, 1995, 6:40**: Clear sky. Poor IR contrast. Still some snow cover on the side of the road.

3. **Jan. 10, 1995, 5:55**: Clear sky and light snow cover. Thermal contrasts are relatively poor but sufficient to see most AT and AP buried mines.

4. **Jan. 11, 1995, 5:45**: Overcast, medium heavy ground fog, light wind and frost on the road. Even in these weather conditions, a light contrast is observed, which is sufficient to detect almost the totality of the buried mines.

5. **Jan. 12, 1995, 5:55**: Overcast day and breezy. A situation of poor IR contrast.

6. **Jan. 16, 1995, 5:40**: Overcast day and 2.5 inches of fresh snow on the road. No thermal contrast are observable and almost no false alarm for the whole road (very flat image).

7. **Jan. 19, 1995, 5:50**: Light overcast day with light wind. Poor thermal contrast observed. Only the mines detected are those having the tire print over them. Also, few occurrences of positive contrasts.

8. **Jan. 23, 1995, 6:26**: Very light ground fog. Medium IR contrasts observed after back blading the road. Still a few centimetres of compacted snow left on the side of the road.

9. **Jan. 24, 1995, 5:40**: Clear day with light breeze. A pass with a good IR contrast. Once again, the snow cover seems to help reduce false alarms.

INTERNAL DISTRIBUTION

DREV R–9615

1 – Deputy Director General
1 – Chief Scientist
1 – H/ASSTA
1 – H/PSSTA
6 – Document Library
1 – J.-R. Simard (author)
1 – D. Bonnier
1 – V. Larochelle
1 – J. Dumas
1 – R. Fortin
1 – J. Bedard
1 – L. Sévigny
1 – P. Chevrette
1 – D. St-Germain
1 – L. Bissonnette

UNCLASSIFIED

EXTERNAL DISTRIBUTION

DREV R–9615

2 – DRDIM
1 – CRAD
1 – D Mil E 4
1 – D Mil E 4-5
1 – DSAL 5 Doug Wakefield

DRES:
9 – Attn: Maj. Al Carruthers
– CWO Bill MacLean
– Dr. John Evans
– Dr. John McFee
– Dr. Yoga Das
– Dr. Vic Aitken
– Mr. Kevin Russell
– Mr. Wayne Sirovyak
– Mr. Blair Cain

DREO:
2 – Attn: Dr. Benny Wong
– Dr. Shyam Khanna

1 – Mr. David Green
Computing Devices Canada
P.O. Box 8508
Ottawa, ON
K1G 3M9

1 – Dr. Wilson So
Communications Systems Division
1020-68th Avenue N.E.
Calgary, AB
T2E 8P2

UNCLASSIFIED
SECURITY CLASSIFICATION OF FORM
(Highest classification of Title, Abstract, Keywords)

DOCUMENT CONTROL DATA

1. ORIGINATOR (name and address) Defence Research Establishment Valcartier P.O. Box 8800 Courcelette, P.Q. Canada G0A 1R0	2. SECURITY CLASSIFICATION (Including special warning terms if applicable) UNCLASSIFIED

3. TITLE (its classification should be indicated by the appropriate abbreviation (S,C,R or U)
Theoretical and Experimental Characterizations of the IR Technology for the Detection of Low-Metal and Nonmetallic Buried Landmines (U)

4. AUTHORS (Last name, first name, middle initial. If military, show rank, e.g. Doe, Maj. John E.)

Jean-Robert Simard

5. DATE OF PUBLICATION (month and year)	6a. NO. OF PAGES	6b. NO. OF REFERENCES
	104	16

7. DESCRIPTIVE NOTES (the category of the document, e.g. technical report, technical note or memorandum. Give the inclusive dates when a specific reporting period is covered.)

Technical Report

8. SPONSORING ACTIVITY (name and address)

CRAD

9a. PROJECT OR GRANT NO. (Please specify whether project or grant)	9b. CONTRACT NO.
D6300	

10a.ORIGINATOR'S DOCUMENT NUMBER	10b. OTHER DOCUMENT NOS.
R-9615	N/A

11. DOCUMENT AVAILABILITY (any limitations on further dissemination of the document, other than those imposed by security classification)

- [X] Unlimited distribution
- [ ] Contractors in appoved countries (specify)
- [ ] Canadian contractors (with need-to-know)
- [ ] Government (with need-to-know)
- [ ] Defence departments
- [ ] Other (please specify) :

12. DOCUMENT ANNOUNCEMENT (any limitation to the bibliographic announcement of this document. This will normally correspond to the Document Availability (11). However, where further distribution (beyond the audience specified in 11) is possible, a wider announcement audience may be selected.)

UNCLASSIFIED
SECURITY CLASSIFICATION OF FORM

UNCLASSIFIED
SECURITY CLASSIFICATION OF FORM

13. ABSTRACT (a brief and factual summary of the document. It may also appear elsewhere in the body of the document itself. It is highly desirable that the abstract of classified documents be unclassified. Each paragraph of the abstract shall begin with an indication of the security classification of the information in the paragraph (unless the document itself is unclassified) represented as (S), (C), (R), or (U). It is not necessary to include here abstracts in both official languages unless the text is bilingual).

One of the greater threat during peacekeeping operations is buried low-metal mines on communication roads. The Department of National Defence (DND) of Canada, as many other equivalent organizations around the world, initiated important efforts to develop a multi-sensor teleoperated mine detection vehicle, the Improved Landmine Detection Capability (ILDC) program, to solve this problem. One of the sensor evaluated for this program is the IR imaging technology. This document reports the results of many trials performed during the last 1 1/2 years and models developed from these results to characterize the capabilities of this technology. The fundamental variables dictating the formation of the buried mine IR signature are identified and a monitoring technique predicting the optimum performance of the technology is proposed. From especially designed trials to simulate the scenarios addressed by the ILDC program, the detection efficiencies and the false alarm rates on packed gravel and sand roads at different times of the day are measured. From these results, it is observed that the best performances are obtained at night and on packed gravel road. In addition, the performances of the technology under winter alike weather, on shady roads, and for many other external conditions of interest for the ILDC program are investigated.

14. KEYWORDS, DESCRIPTORS or IDENTIFIERS (technically meaningful terms or short phrases that characterize a document and could be helpful in cataloguing the document. They should be selected so that no security classification is required. Identifiers, such as equipment model designation, trade name, military project code name, geographic location may also be included. If possible keywords should be selected from a published thesaurus. e.g. Thesaurus of Engineering and Scientific Terms (TEST) and that thesaurus-identified. If it is not possible to select indexing terms which are Unclassified, the classification of each sould be indicated as with the title.)

IR
infrared
detection
buried
landmine
low-metal
nonmetallic
passive
LWIR
MWIR
temperature
gradient
road
gravel
packed
sand

S02142

UNCLASSIFIED
SECURITY CLASSIFICATION OF FORM

(DCD03E.IFD - 95.02.22)